ULTRA-SMALL GOLD NANOPARTICLES BY GALVANIC REPLACEMENT OF LARGER SILVER NANOPARTICLES

by

CHANG-TING LIN

Presented to the Faculty of the Graduate School of

The University of Texas at Arlington in Partial Fulfillment

of the Requirements

for the Degree of

MASTER OF SCIENCE

THE UNIVERSITY OF TEXAS AT ARLINGTON

May 2019

ACKNOWLEDGMENT

I want to thank everyone who has helped me during the past two years, but first I want to send my gratitude to my advisor Dr. Yaowu Hao for his guidance and patience for me to learn many things about nanotechnology and finish my thesis. I would also like to thank my colleagues especially Shahab Ranjbar Bahadori who always provided courage and supports.

I am also grateful to the great team in the Radiology Department of UT Southwestern Medical Center in Dallas, Aditi Mulgaokar who significantly contributed to this study. I especially appreciate Dr. Xiankai Sun, whose knowledge and support help this work possible.

Finally, I would like to thank my family in Taiwan. They always give me endless support and encouragement for me to finish my master's degree.

ABSTRACT

ULTRA-SMALL GOLD NANOPARTICLES BY GALVANIC REPLACEMENT OF LARGER SILVER NANOPARTICLES

Chang-Ting Lin, MS

The University of Texas at Arlington, 2019

Supervising Professor: Yaowu Hao

In the last two decades, Au nanoparticles have been extensively explored for their biomedical applications, which is mainly driven by their biocompatibility and special optical properties known as surface plasmon resonance (SPR) effect. A variety of Au nanoparticles with different sizes and shapes have been synthesized and tested both in vitro and in vivo. For in vivo applications, it is usually required that Au nanoparticles can be cleared through urine (renal clearance). Renal clearance is determined by several factors of Au nanoparticles, including size, shape and surface modification.

In this thesis, for the purpose of using Au nanoparticles as carriers to carry radioactive isotopes such as Cu-64 or Pd-103 into human body for cancer imaging and treatment, we developed a process to synthesize, functionalize and be labelled with Cu of ultra small Au nanoparticles.

We developed an easy and fast way to synthesize ultra small Au nanoparticles with an average diameter less than 5 nm using galvanic replacement reaction to replace spherical Ag nanoparticles with Au chloroaurate. This synthesis process can be completed within an hour at room temperature. To ensure the renal clearance property, Au nanoparticles with size less than 2 nm have been successfully isolated from synthesized Au nanoparticles.

The renal clearance of the nanoparticles are also strongly related to the surface chemistry of the nanoparticles. The Ag nanoparticles we used for the synthesis of Au nanoparticles have polyvinylpyrrolidone (PVP) coating on the surface. PVP is not an ideal surface coating for renal clearance.

Therefore, we first introduced a simple way to remove the PVP coating by washing the particles with acetone. Then the surface of the Au nanoparticles was functionalized with glutathione which has been proven to be a good surface coating for renal clearance.

In addition, we have incorporated Cu on to the surface of these Au nanoparticles using the electroless deposition process, creating a protocol for the radiolabeling of Au nanoparticles.

TABLE OF CONTENTS

LIST OF FIGURES

LIST OF TABLES

1. INTRODUCTION

Au nanoparticles have been used for many years in human history; the first usage of Au nanoparticles can date back to ancient Rome. In 1900's, the synthesis method of Au nanoparticles were already well-developed. Since Au are inert to the human body, this makes Au nanoparticles an ideal candidate for in vivo applications such as labeling, delivering, and sensing. However, for Au nanoparticles to be used in the clinical practice, because the United States Food and Drug Administration (FDA) required all injected drugs to be renal clearable and have to be cleared from the human body within a reasonable amount of time, Au nanoparticles have to be renal clearable. Researches have proved that nanoparticles with hydrodynamic diameter less than 6 nm and with a positive surface charge can pass through the kidney filtration barrier easily. Thus, in this thesis, we introduced a facile method to synthesize Au nanoparticles with a diameter less than 5 nm and with an ideal surface coating. These Au nanoparticles are proposed to be used as carrier to carry radioactive isotopes for cancer imaging and treatments.

First, we developed a simple way to synthesize Au nanoparticles smaller than 5 nm by galvanic replacement of larger Ag nanoparticles, which is an electrochemical process that is driven by the reducing potential between two different metals. Because Au has a higher reducing potential, it can oxidate the Ag atom and get reduced on the Ag nanoparticles. Also, due to that Au ions used in this reaction has three positive charges and resultant Ag ion only has one positive charge, one Au atom can replace three Ag atoms so that the charge balance can be achieved. Therefore, when Au atoms replace all the Ag atoms, the particles size reduced. In our case, the Ag nanoparticles we purchased has an average diameter of around 7 nm, after the replacement reaction the diameter of Au nanoparticles decrease to less than 3 nm.

Since the purchased Ag nanoparticles were coated with polyvinylpyrrolidone (PVP), which is not the best surface coating for renal clearable nanoparticles, so the next step is to remove this coating and replace with another coating, glutathione, which has been proved to be a good surface coating for renal clearance. PVP coating were removed by simply washing nanoparticles with acetone. The zeta potential of the Au nanoparticles before and after the acetone wash was -11.12 mV and -33.12 mV respectively,

indicated that the original surface coating on the Au nanoparticles was removed. After the coating was removed, we functionalized the naked Au nanoparticles with glutathione and the zeta potential was measured again. The result shows that the zeta potential increased from the -33.12 mV to -16.06 mV after coating the particle with glutathione, this confirms the glutathione was successfully coated on the surface of the Au nanoparticles.

Although the Au nanoparticles we synthesized were tiny, the size distribution was not very uniform; it contains particles ranging from 1.5 nm to 7 nm. We developed a process to isolate the 2 nm Au nanoparticles so that it has much better renal clearance properties. we used a 50K Amicon filter device to isolate the particles that were less than 2 nm. The size distribution of the isolated Au nanoparticles was uniform, and there is no Au nanoparticles larger than 3.5 nm in the filtered samples.

Finally, since we want to use our Au nanoparticles as a carrier to carry radioactive isotopes such as Cu-64 to the cancer sites, we tried to incorporate Cu on the Au nanoparticle surface via electroless deposition. Electroless deposition is an electrochemical process. Unlike electrodeposition, it does not require any external power source. Electroless deposition needs three components: a catalytic substrate, a reducing agent, and a metal salt solution. Here we use Au nanoparticles as the catalytic substrate, formaldehyde as the reducing agent, and Cu sulfate as the metal salt. During the reaction, the metal ions (Cu ions) near the surface of the catalytic substrate (Au nanoparticles) combine with the electron provided by reducing agent (formaldehyde) and form the Cu lattice on the surface of the catalytic substrate of Au nanoparticles. From the inductively coupled plasma mass spectrometry, we confirm the existence of the Cu on the surface of the Au nanoparticles.

In the following chapters, the background information about the history, synthesis methods of the Au nanoparticle, and the brief explanation of renal clearance are discussed in chapter 2. The detailed synthesis method and the surface functionalization method of the Au nanoparticles are described in chapter 3. The process to incorporate Cu to the Au nanoparticles by electroless deposition is discussed in detail in chapter 4. Finally, the conclusion is summarized in chapter 5.

2. BACKGROUND INFORMATION

2.1 Au Nanoparticles

Since 2001, the National Nanotechnology Initiative has received more than $21 billion of investment cumulatively [1] and the market share of the products incorporating nanotechnology was projected to surpass $3 trillion by 2020 [2], this is because the nanoscience and nanotechnology have demonstrated great potential in many scientific and industrial advance. Due to the unique optical property known as the surface plasmonic resonance (SPR), which is an optical phenomenon arising from the interaction between the conduction electrons in the metal and the electromagnetic field, nanoparticles made by noble metal especially for Au and Ag nanoparticles have been investigated heavily in various application such as biomedicine [3,4], sensing [5,6], and bio-imaging contrast agent [7,8]. Numerous researches have reported that the Au nanoparticles are renal clearable and useful for clinical application including labeling, delivering, and sensing. It is also been reported that Au nanoparticles functionalized with glutathione have low immunogenicity, clearance times, and biocompatibility, make it an ideal candidate for in vivo application [9].

Many methods have been developed to synthesize different size of Au nanoparticles and their in vivo applications and research and toxicity have extensively been reported. In this section, the history and the synthesis method of Au nanoparticles were described. The properties and the synthesis of ultra-small Au nanoparticles were discussed.

2.1.1 History of Au Nanoparticles

The usage of Au nanoparticles can date back to 4th-century; it was used in a Roman glass cage cup known as the Lycurgus cup (figure 2.1) (which is part of the collection of British Museum), in which it can show two different colors depend on the placement of the light source. When there is no light passing through the glass of the cup, the color of the cup will be green (figure 2.1a). When the light transmitted through the cup, the color will change from green to red (figure 2.1b). This dichroic effect is attributed to

the fact that due to the glass contains many Ag-Au alloy nanoparticles with a diameter around 70 nm. When the light passes through the glass, it will be scattered by these Ag-Au alloy nanoparticles [10]. But it was until the 1850s, the first synthesis process of Au nanoparticles was reported. In 1857, Michael Faraday used phosphorus as reducing agent to reduce the Au chloride solution and successfully produced ruby colored aqueous colloidal Au nanoparticles solution [11]. Since then, different synthesis methods have been reported to synthesize Au nanoparticles with different sizes and shapes.

Figure 2. 1 The Lycurgus cup in a) the reflected light and b) transmitted light [12]

2.1.2 Synthesis Methods of Au Nanoparticles with Different Sizes or Shapes

Due to the size and shape of the Au nanoparticles are strongly related to the SPR properties, different methods have been developed to synthesize different size or shape of Au nanoparticles. Citrate reduction method is proved to be an easy method to produce Au nanoparticles [13]. By using citrate to reduce Au chloroaurate ($HAuCl_4$), Au nanoparticles with different size can be achieved. It has been demonstrated that the SPR peak of the spherical Au nanoparticles with a diameter between 40 to 100 nm is

at around 530 to 560 nm. To synthesize Au nanorods, the electro-templated [14], photochemical method [15], and seed-mediated method [16] was developed. The SPR effect of the Au nanorods changes depending on their orientation with the incident light. The SPR peak at 530 nm corresponds to the horizontal plasmon oscillation and a stronger SPR peak at near-infrared region emerge from the plasmon oscillation along the longitudinal axis of the nanorods [17]. Au nanocages can be produced by using the galvanic replacement reaction to replace Ag nanocube with $HAuCl_4$ [18]. Based on the inner edge length of the Au nanocages, the SPR peak can be tuned between 710 nm to 810 nm when the inner edge length is between 30 nm to 45 nm. The so-called Au nanoshell can be synthesized by deposit Au on to the silica colloidal surface [19] and it was found that the SPR peak has a strong dependence on the void size and wall thickness. For aqueous suspended Au nanoshells with a thinner wall (~ 2 nm), it has an SPR peak at around 720 nm. In this thesis, we demonstrate a simple method to synthesize small spherical Au nanoparticles by using galvanic replacement reaction, the synthesis method will be discussed in detail later on. The ultraviolet-visible spectroscopy (UV-Vis) was utilized to record the SPR effect of the Au nanoparticles and we got the SPR peak of our Au nanoparticles is at around 520 nm.

2.1.2.1 Au Nanosphere

The most frequently applied method to synthesize spherical AuNPs is the citrate reduction method, which was introduced by Turkevitch in 1985 [20]. The reaction of using citrate to reduce Au chloroaurate ($HAuCl_4$) in water is presented as follows:

$$\boldsymbol{6AuCl_4^- + C_6H_8O_7 + 5H_2O \rightarrow 6CO_2 + 24Cl^- + 6Au + 18H^+}$$

The particles' size can be controlled by adjusting the concentration of the citrate. In 1994, M. Brust introduced a method that can produce 1-3 nm Au nanoparticles with a thiol surface coating using two-phases (water-toluene) reaction of $AuCl_4^-$ with sodium borohydride in the presence of alkanethiol. Since the strong affinity between Au and sulfur [21], the thiol ligands can bind with Au and functionalize the

surface of the Au nanoparticle. This allowed the production of more stable Au nanospheres. The overall reaction is summarized below:

$$AuCl_{4\,(aq)}^{-} + N(C_8H_{17})_4 + (C_6H_5Me) \rightarrow N(C_8H_{17})_4 + AuCl_4 - (C_6H_5Me)$$

$$mAuCl_{4\,(aq)}^{-} - (C_6H_5Me) + nC_{12}H_{25}SH(C_6H_5Me) + 3me^{-}$$
$$\rightarrow 4mCl_{(aq)}^{-} + (Au_m)(C_{12}H_{25}SH)_n(C_6H_5Me)$$

Here $AuCl_4^-$ is transferred to toluene using tetraoctylammonium bromide ($C_{32}H_{68}BrN$) as the phase-transfer agent and reduced by $NaBH_4$ in the presence of dodecanethiol ($C_{12}H_{25}SH$).

2.1.2.2 Au Nanorod

The synthesis of metal nanowire was first demonstrated in the 1960s, but it was until mid-1990s that chemists developed a facile synthesis process for colloidal metal nanorods. The Au nanorods have attracted the most attention [22] since their plasmonic properties can be tuned by their dimensions [23]. An electro-templated and photochemical [24] method has been developed by Yu, in which a Au metal plate and a platinum plate act as the anode and the cathode respectively; both plates are placed in a solution containing a cationic surfactant, hexadecyltrimethylammonium bromide (CTAB), and a rod-inducing cosurfactant. During the synthesis, the Au metal plate is converted from anode to the platinum plate and form Au nanoparticles on the interfacial surface of the platinum plate. The shape of the Au nanorods is controlled by the CTAB since it serves as a stabilizer to prevent further growth of the nanoparticles. This approach can produce Au nanorods with an approximate dimension of 60 × 10 nm (Figure 2.2).

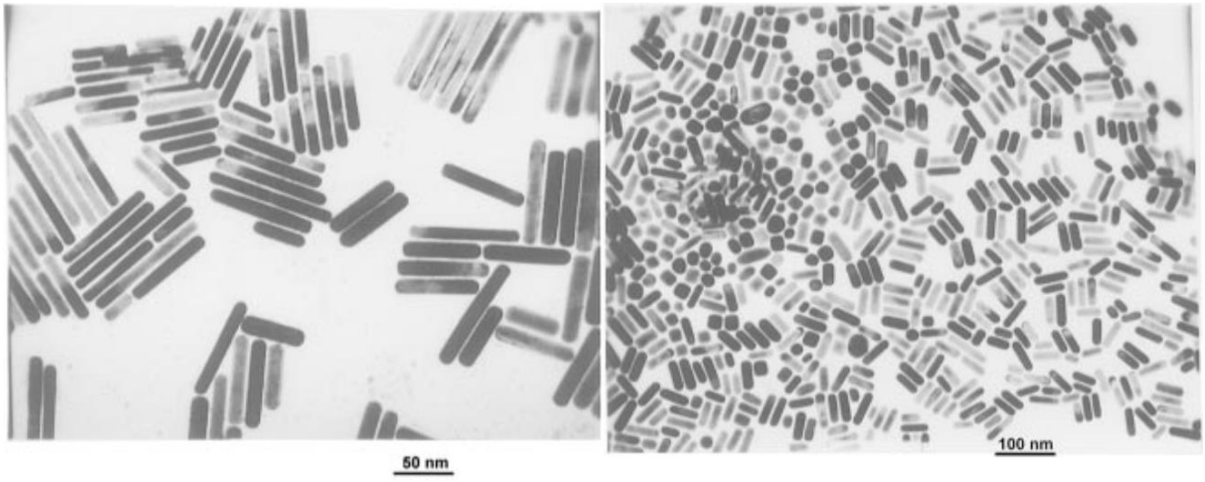

Figure 2. 2 TEM images of Au nanorods with different aspect ratio: 7.6 (left) and 2.6 (right). [24]

In 2001, the seed-mediated growth method was introduced by Jana et al. [25] They prepare rough spherical Au nanoparticles with the diameter around 3 - 4 nm as the seed first, and then mixed the Au nanoparticles solution with a growth solution containing Au salt, rod-shaped micellar template, ascorbic acid, and some Ag ions, in which ascorbic act as the reduction agent and Ag ion is for shape induction. Depending on the Au seed to the Au salt ratio, the aspect ratio of the Au nanorods can be tuned between 1 to 10. (figure 2.3)

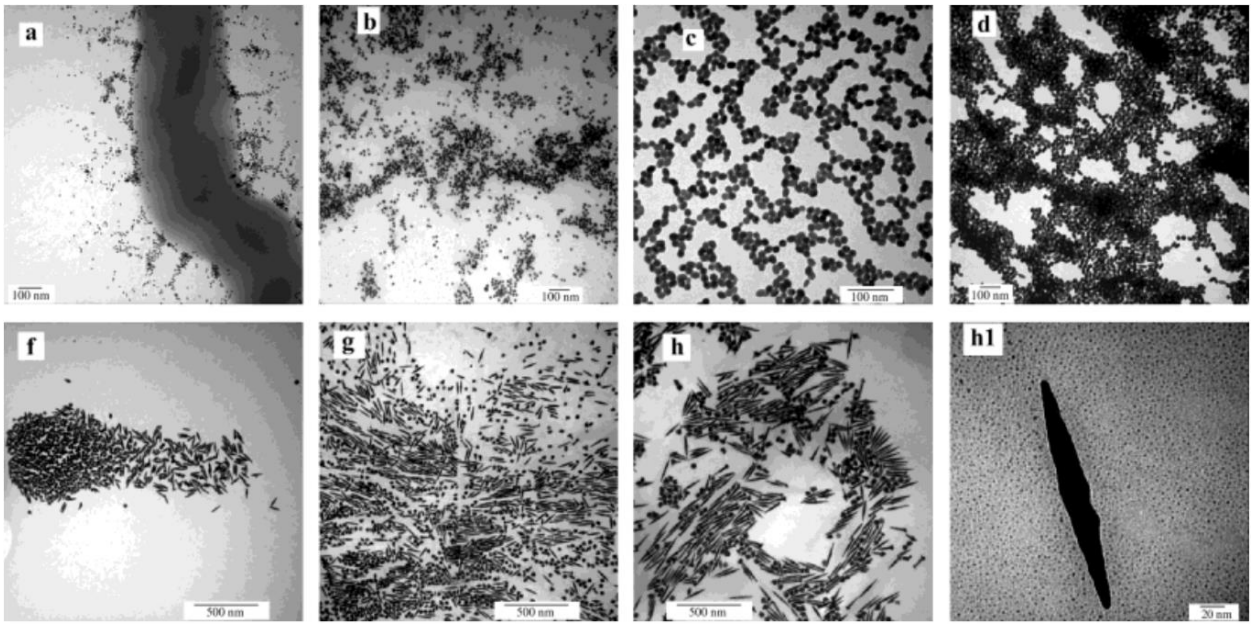

Figure 2. 3 Representative electron micrographs of Au nanoparticles and nanorods corresponding to the spectra a±h in Figure 1. Considering only the spheroids and rods, the average aspect ratios of the particles are 1.5, 2.4, 6.1, 8.0, and 10.0 for sets c, d, f, g, and h, respectively. The particles in sets a and b are nearly spherical and have aspect ratios very close to 1.0. [25]

2.1.2.3 Au Nanocage

The synthesis of Au nanocages was reported by Skrabalak et al. in 2008 [26]. Using Ag nanocubes as a template and $HAuCl_4$ as the precursor, the Au epitaxially deposited on the corner of the Ag nanocages first and gradually adopting the cubic structure. The reaction is driven by the galvanic replacement reaction since the Au has a higher reduction potential than Ag; the reaction can be summarized as follows:

$$3Ag_{(s)} + HAuCl_{4\,(aq)} \rightarrow Au_{(s)} + 3AgCl_{(s)} + HCl_{(aq)}$$

this reaction allows the production of hollow, porous Au nanocages with a dimension less than 100 nm as shown in figure 2.4.

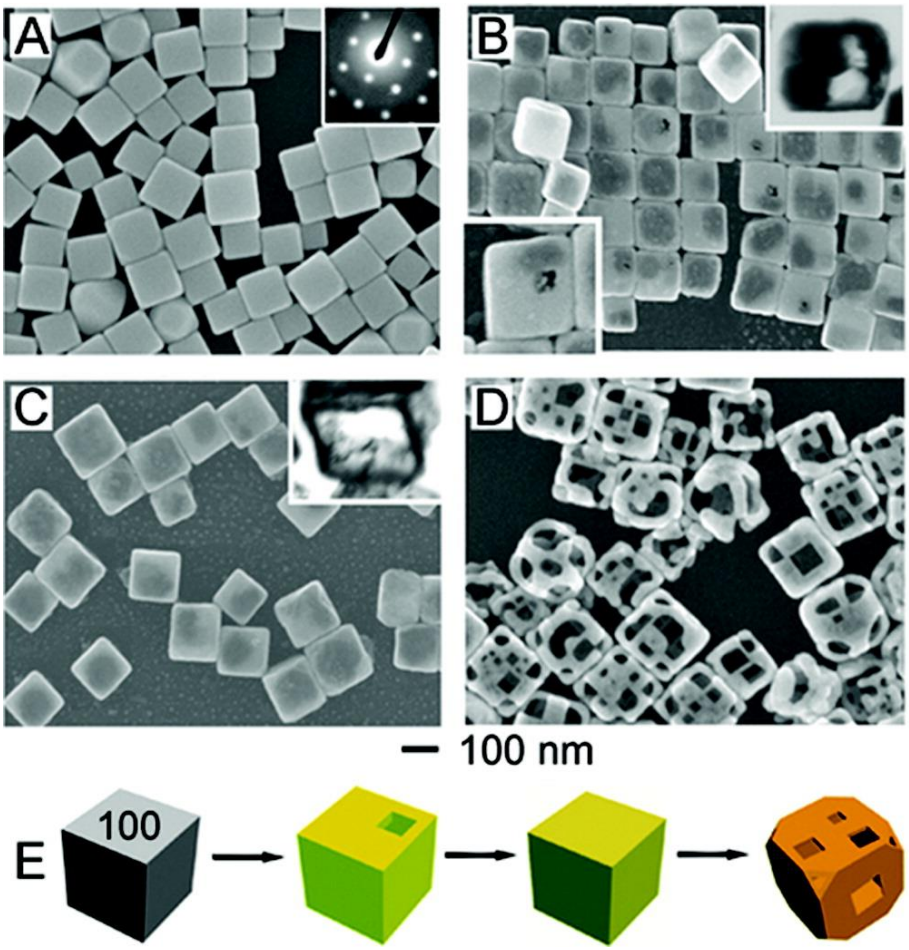

Figure 2. 4 (A) SEM of Ag nanocubes. Inset: electron diffraction indicates they are single-crystals. (B) SEM of the product after 0.30 mL of 1 mM HAuCl4 solution was added to a 5-mL 0.8 mM Ag nanocube suspension; a pinhole (lower inset) is observed on the exposed face of ~1 in 6 nanocubes. Upper inset: TEM of a microtomed sample reveals early hollowing out. (C) SEM of the product after 0.50 mL of HAuCl4 solution was added. Inset: TEM of a microtomed sample reveals the hollow interior of the nanobox. (D) SEM of the product after 2.25 mL of HAuCl4 solution was added. Porous nanocages produced. (E) Illustration summarizing morphological changes. Coloration indicates the conversion of an Ag nanocube into an Au/Ag nanobox then a predominately Au nanocage. [26]

2.1.2.4 Au Nanoshell

Au nanoshells were first demonstrated by Oldenburg et al. [27] with depositing Au on to the silica colloidal surface. First, the surface of the silica nanoparticles was modified with a monolayer of amino-terminated silica and the Au shell is grow on the silica nanoparticles' surface via the seed-mediated electroless plating. The thickness of the Au shell is controlled by adjusting the amount of silica nanoparticle and the Au salt solution. This approach can achieve the production of Au nanoshell with a thickness of 5 - 30 nm. (Figure 2.5)

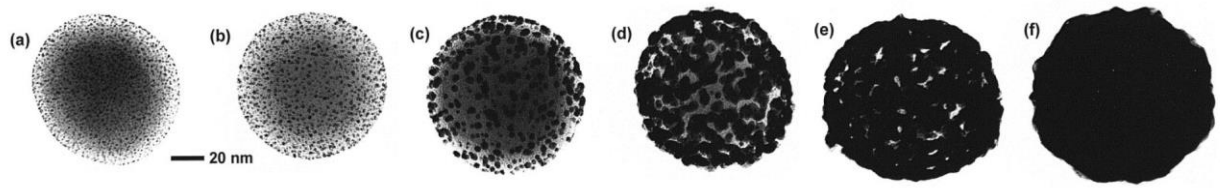

Figure 2. 5 (a)–(f) TEM images of nanoshell growth on 120 nm diameter silica dielectric nanoparticle. (a) Initial Au colloid-decorated silica nanoparticle. (b)–(e) Gradual growth and coalescence of Au colloid on the silica nanoparticle surface. (f) Completed growth of metallic nanoshell. [27]

2.1.2.5 Au Nanoplate

The latest method to synthesize Au nanoplate was reported by Yang et al. [28] which can produce the Au nanoplates with {111} orientation and thickness ranging between 13 nm to 40 nm. (Figure 2.6) After mixing well disperse aqueous AO-2 graphene power solution with the Au precursor (either pure Potassium tetrabromoaurate(III) hydrate ($KAuBr_4$) or $KAuBr_4$ and $HAuCl_4$ mixture) and being heated to 80ºC for a period of time, the product is collected by centrifuge and washed with the deionized water. A different dimension of the Au nanoplates can be achieved by adding a different amount of $HAuCl_4$ or $KAuBr_4$ solution.

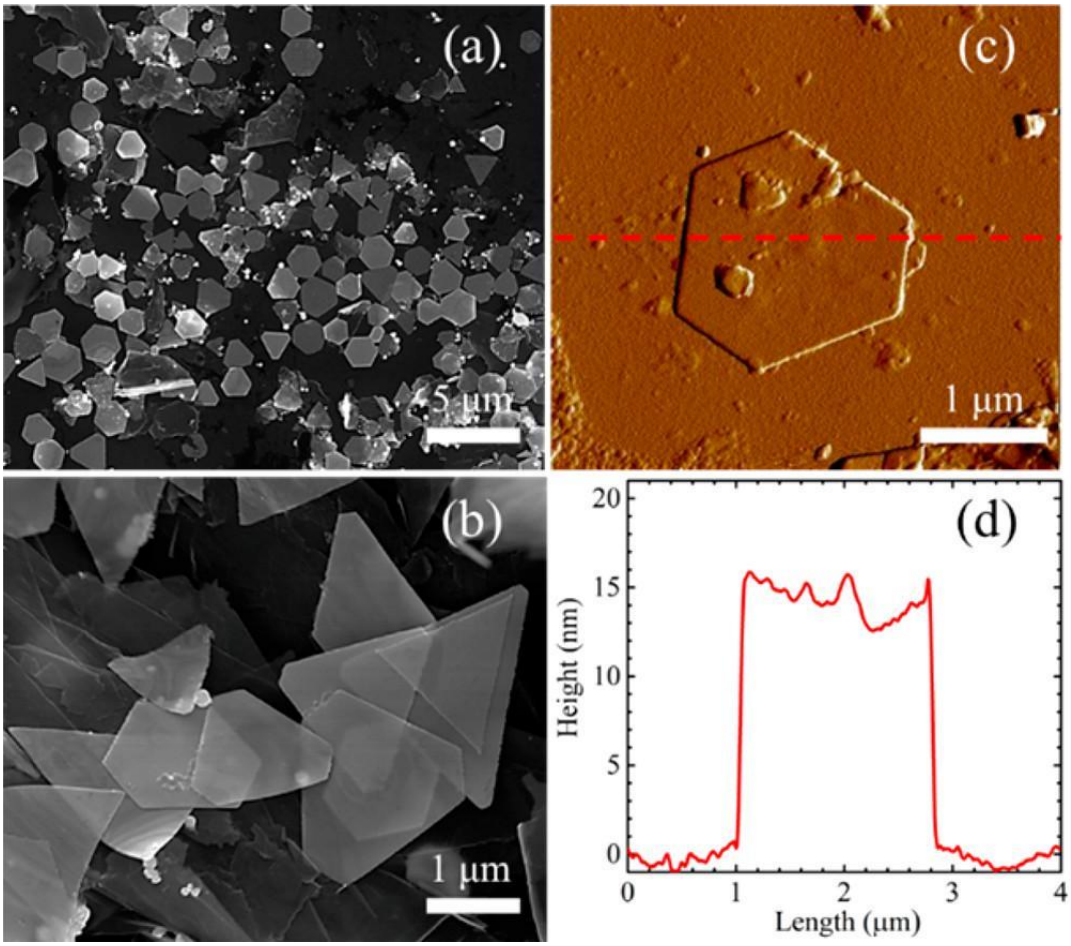

Figure 2. 6 Morphological characterization of Au nanoplates on multilayer graphene is grown with KAuBr4 as the Au precursor. The synthesis time t is 5 h. (a, b) Representative scanning electron microscopy (SEM) images of Au nanoplates on multilayer graphene. (c) Typical atomic force microscopy (AFM) image of an Au nanoplate supported on an oxidized Si(001) substrate. The nanoplate edge contrast is enhanced for clarity. (d) Surface height profile measured along the red dashed line in panel c [28].

2.1.3 Ultra Small Au Nanoparticles

When a nanoparticle smaller than 2 nm which consists of only a few to a hundred atoms, it exhibits some different properties comparing to larger nanoparticles such as strong photoluminescence, large Stokes shift and high emission rate [29]. They are usually referred as the nanocluster. For nanocluster made of Au atoms, it has shown some great potential in theoretical studies and practical applications since Au nanoclusters have good water solubility, low-toxicity, biocompatibility, and ease of surface functionalization [30].

2.1.3.1 Optical Property of Au Nanocluster

The optical property of Au nanoparticle mostly arises from the resonant oscillation of the conduction electrons on their surface stimulated by the incident electromagnetic wave, also known as the surface plasmon resonance. As the diameter of the nanoparticle decrease to nanocluster, the surface of the nanocluster is too small to support the plasmon, instead, it forms continuous states like a conductor, exhibiting discrete energy levels. For instance, Zhu et al. [31] have demonstrated that glutathione-coated Au_{25} nanoclusters show several distinguish absorption features in the range of 400-1000 nm. It is also been reported that the absorption peaks tend to have a blue shift when the size decrease due to the spacing between the discrete states in each band increases [32].

2.1.3.2 Synthesis Method of Au Nanoclusters

There are many synthesis methods of Au nanocluster have been reported, a few similarities can be spotted. In order to synthesis small Au nanoclusters, weak reducing agents have to be used. Also, to prevent the aggregation of these Au nanoclusters, thiol-containing molecules are required as the reducing agent and stabilizer.

Yue et al. [33] have demonstrated a one-step microwave-assisted synthesis of highly fluorescent Au nanocluster by using bovine serum albumin (BSA), where BSA is reacting with $HAuCl_4$ under basic condition (pH 12) at 37ºC by using microwave irradiation to maintain the temperature. The nucleation and

growth can be controlled easily by using microwave irradiation as a heat source since the dielectric contains the solvent and the reactant, and selective dielectric heating can provide significant enhancement in the transfer of energy directly to the reactants, which can increase the internal temperature instantly. As a result, they showed that microwave-assisted synthesis is an effective method to produce stable, protein-protected Au nanoclusters composed of as few as 16 atoms from a BSA-$HAuCl_4$ solution.

2.2 Renal Clearable Nanoparticles

For in vivo applications of inorganic nanoparticles, due to long term accumulation in the body may cause some potential health issue, the Food and Food and Drug Administration (FDA) requires the injected drug into the human body have to be cleared out from the body in a reasonable period of time [34]. Therefore, to make the nanoparticles renal clearable has become a priority for inorganic nanoparticles to be translated into the clinical practices.

2.2.1 Introduction to Renal Clearance

Renal clearance is a measurement to evaluate the function of the kidney; it varies with different substances and it tells about the amount of substance got filtered out from the blood plasma through the kidney filtration system. The kidney filtration system is consisted of million tiny filters called kidney corpuscles, each kidney corpuscles has glomerular capillaries and a glomerular capsule known as Bowman's capsule (figure 2.7). When the blood plasma entered the glomerulus through the afferent arteriole, some portion of the blood plasma will be filtered through the glomerular filtration barrier into the Bowman's space and enter the peritubular tubule where reabsorption and secretion will take place (figure 2.7). The blood plasma that did not get filtered through the glomerulus will travel via efferent arteriole to peritubular capillaries where reabsorption and secretion will take place between the proximal tubule and peritubular capillaries. The substance which passes through the filtration barrier and enters the proximal tubule will eventually get excreted and carrier out from the body in urine [35].

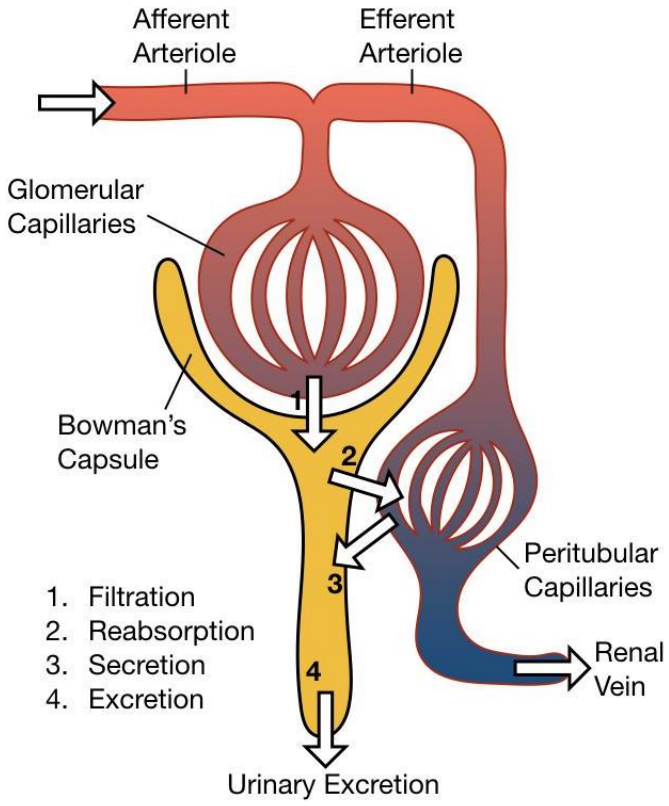

Figure 2. 7 Schematic of the physiology mechanism of the kidney.

2.2.2 Properties affecting the renal clearance

The glomerular capillary barrier is made of three layers: endothelium, glomerular basement membrane, and podocyte extension (shown in figure 2.8c). Each layer has different sizes of pores that allow the water-soluble substance to enter Bowman's space. In order to let an inorganic nanoparticle to exit the kidney, it has to pass through the endothelium (with pore diameter between 70 ~ 90 nm), glomerular basement membrane (with 4 ~ 11 nm of pores), and podocyte extension (with 4 ~ 11 nm of filtration slit). Because of the combination of these three layers, whether or not a particle can pass through the glomerular capillary barrier and metabolize is related to the particle's size, shape, and its surface chemistry [36]. Numbers of research have been reported that the nanoparticle with a hydrodynamic diameter (HD) small than 6 nm can easily filter through the glomerular capillary barrier, whereas it is difficult for particle HD

larger than 8 nm to pass the barrier. The particles HD between 6 ~ 8 nm depending on both size and surface charge of the particle. Also, not only spherical nanoparticle can pass the glomerular capillary barrier, but also the nanostructure with the cylindrical shape and diameter smaller than kidney filtration threshold can be renal clearable. The surface charge of the nanoparticle is also affecting kidney filtration. Since the glomerular capillary barrier is negatively charged, it is easy for nanoparticles with the diameter between 6-8 nm with a positive surface charge to pass through the glomerular capillary barrier. However, it becomes difficult for the nanoparticle with a negative charge or neutral surface charge to exit [37].

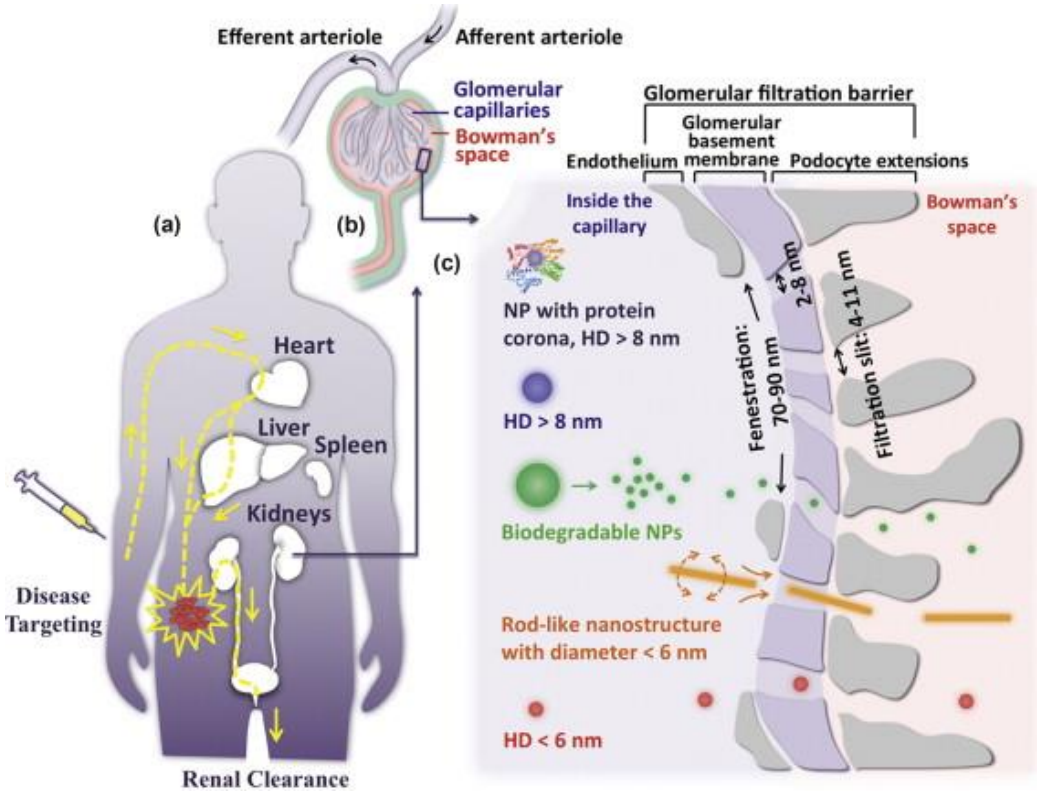

Figure 2. 8 (a) Ideal disease targeting of renal clearable nanoparticles (NPs) in clinical practices: the NPs specifically target the diseases and untargeted ones are rapidly cleared out of the body through the urinary system. (b) The schematic structure of the kidney corpuscle. (c) Glomerular filtration is a nanoscale phenomenon. The glomerular capillary wall is made of three specialized layers: fenestrated endothelium, glomerular basement membrane, and podocyte extensions of glomerular epithelial cells [36].

2.2.3 Renal Clearance of Different Nanoparticles

Numerous of nanoparticles have been reported that they have renal clearance ability. In this section, renal clearable nanoparticles such as iron oxide nanoparticles, silicon oxide nanoparticles, and Au nanoparticles are discussed.

2.2.3.1 Iron Oxide Nanoparticle

Magnetic iron oxide nanoparticles have been used for a wide variety of biomedical applications and more and more iron oxide nanoparticles related to biomedicines have been approved by the FDA for human use. It has been reported that iron oxide nanoparticles smaller than 10 nm have higher chances to be eliminated through the renal clearance. However, iron oxide nanoparticles bigger than 100 nm can be trapped in the liver and spleen through macrophage phagocytosis [38] and cannot be removed via renal clearance. Feng et al. [39] have demonstrated the clearance of three different commercially available iron oxide nanoparticles with different size and surface coating: iron oxide nanoparticles with polyethylene glycol (PEG, MW = 2 kDa) coating (10 nm, SMG-10; 30 nm, SMG-30) and iron oxide nanoparticles with polyethyleneimine (PEI, MW = 25 kDa) coating (10 nm, SEI-10). The physicochemical detail was shown in table 2.1.

Table 2. 1 The physicochemical characteristics of different iron oxide nanoparticles [39]

Iron oxide nanoparticles	Size by TEM (nm)	Hydrodynamic size by DLS (nm)	Zeta potential (mV)
SEI-10	10	17.2 ≦ 5.0	+29.28
SMG-10	10	16.5 ≦ 4.7	-0.52
SMG-30	30	35.8 ≦ 10.3	-0.52

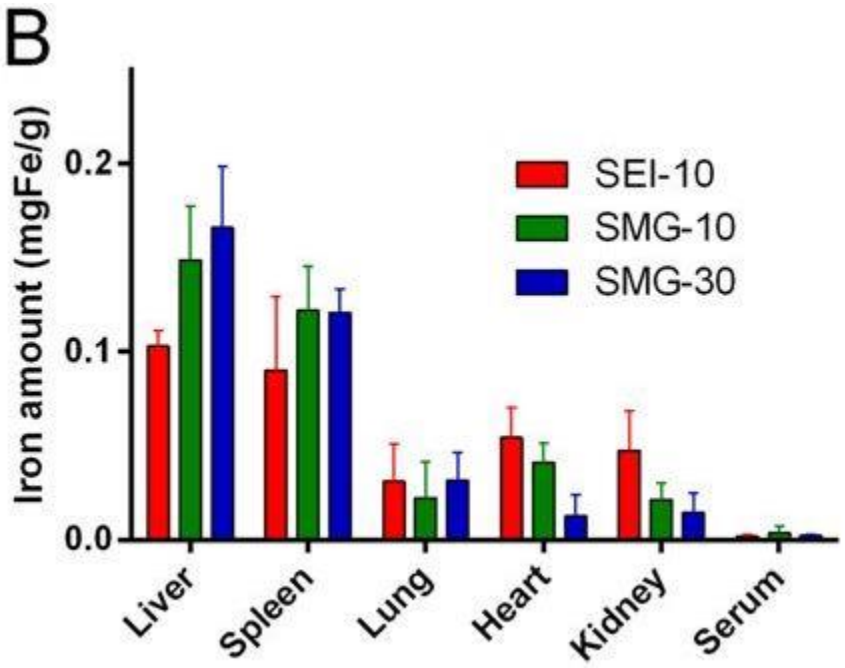

Figure 2. 9 The distribution of IONPs in different organs were quantified by ICP-MS at 24 h post-injection [39].

The clearance of these iron oxide nanoparticles was tested in SKOV-3 tumor-bearing mice. Their investigation (figure 2.9) shows that 24 hours after the injection, these particles tend to be trapped in the organs such as the liver and spleen, with little amount distributed in other organs such as lung, heart, kidney, and serum. They found that the uptake of SEI-10 particles in the kidney was notably higher than SMG-10 and SMG-30, indicating SEI-10 has faster clearance since its surface charge was more positive than others. Also, among the PEGylated iron oxide nanoparticles, SMG-10 shows a higher clearance rate compare with SMG-30, this means small size iron oxide nanoparticle can easily be eliminate by renal clearance.

2.2.3.2 Silicon Nanoparticle

Silicon nanoparticles are also attracted a great amount of researchers' attention due to its biocompatibility [40] and biodegradability [41]. Unlike other inorganic nanoparticles, porous silicon nanoparticles can self-destruct into harmless, renal clearable chemical such as orthosilicic acid ($Si(OH)_4$)

which is the predominant form of silicon that can be absorbed by the human body and it can be found in numerous tissues. Moreover, silicic acid can also be excreted from the body efficiently through the urine [42]. Park et al. [43] have demonstrated the accumulation and degradation of the 126 nm luminescent porous silicon nanoparticles (LPSiNPs) in vivo. They intravenously inject 20 mg/kg of LPSiNPs into the mice and the biodistribution (figure 2.10b) shows that after the injection, the injected LPSiNPs mainly accumulate in the organ such as the liver and spleen initially. After 1 week, the accumulated LPSiNPs in the organ is significantly decreased and completely cleared within 4 weeks. The clearance of LPSiNPs is due to the degradation of silicic acid followed by excretion (figure 2.10a). This result shows a different type of nanostructure with low-toxicity degradation pathway for in vivo application.

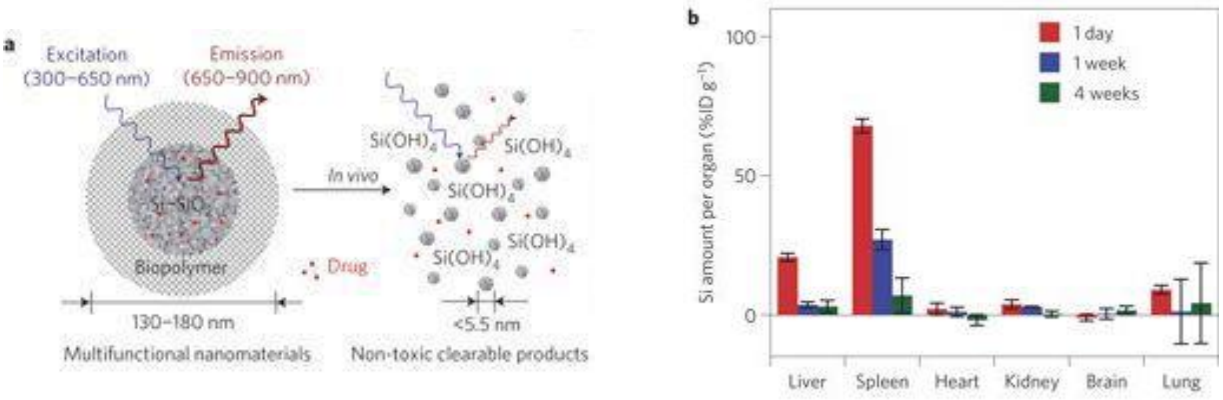

Figure 2. 10 **a)** Schematic diagram depicting the structure and *in vivo* degradation process for the (biopolymer-coated) nanoparticles used in this study. **b)** In vivo biodistribution and biodegradation of LPSiNPs over a period of 4 weeks in a mouse. Aliquots of LPSiNPs were intravenously injected into the mouse (n=3 or 4, dose=20 mg kg−1). The silicon concentration in the organs was determined at different time points after injection using ICP-OES [41].

2.2.3.3 Au Nanoparticle

Au nanoparticles were also one of the desirable nanoparticles that can be used in the clinic application due to its low toxicity [44] to the human body when compared to other inorganic nanoparticles. In addition, the surface of the Au nanoparticles can be easily functionalized to accomplish better clearance

[45]. The clearance and toxicity of glutathione-coated Au nanoparticles were reported by Simpson et al. [46]. The 1.2 nm ± 0.9 nm glutathione-coated Au nanoparticles were prepared in sterile phosphate-buffer saline and injected into mice with different dosage concentration (0 μM, 10 μM, 20 μM, 30 μM, 40 μM, and 60 μM in a 200 μL total volume phosphate-buffer saline), the urine was collected and the mice were euthanized at 3 different time point (24 hours, 2-week, and 4-week) for organ distribution data.

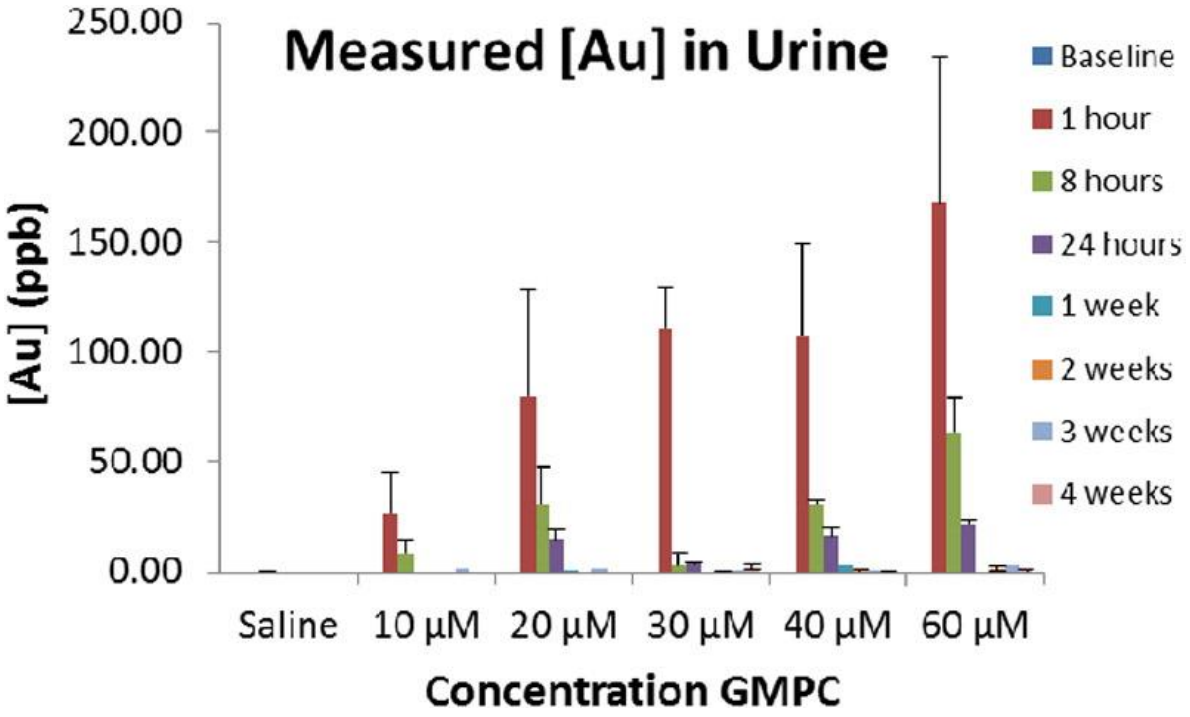

Figure 2. 11 Urinalysis of glutathione-coated Au nanoparticles (n = 5 for each time point, 200 μL injections) shows a significant percentage of particles is cleared through renal filtration within 1 h, continues for up to 24 h and returns to baseline concentrations within 1 week. This indicates the glutathione-coated Au nanoparticles is capable of quick passage into the kidneys and bladder and does not cause a strain on the renal system as the injection concentration is increased. (ICP-MS detection limit = 0.4 ppb). Baseline time points (taken before injection) were essentially 0 ppb at all concentrations [46].

The Urinalysis (figure 2.11) determined by inductively coupled plasma mass spectrometry (ICP-MS) shows that for all concentration of injected AuNPs, more than 30% of particles were cleared through the renal system within 1 hour and more than 60% was excreted within 8 hours. After 24 hours, almost all of the injected Au nanoparticles can be cleared via kidneys and bladder. The concentration of Au in the urine returned to baseline level within a week for all injection concentration, this meant that the glutathione-coated Au nanoparticles were capable to pass through the kidneys and bladder. In the entire 6-week of study, there was no sign of illness, stress, or discomfort of the mice injected with the glutathione-coated Au nanoparticles. In addition to the urinalysis, biodistribution of glutathione-coated Au nanoparticles was also investigated (Figure 2.12) in three different time frames (24-hours, 2-week, and 4-week).

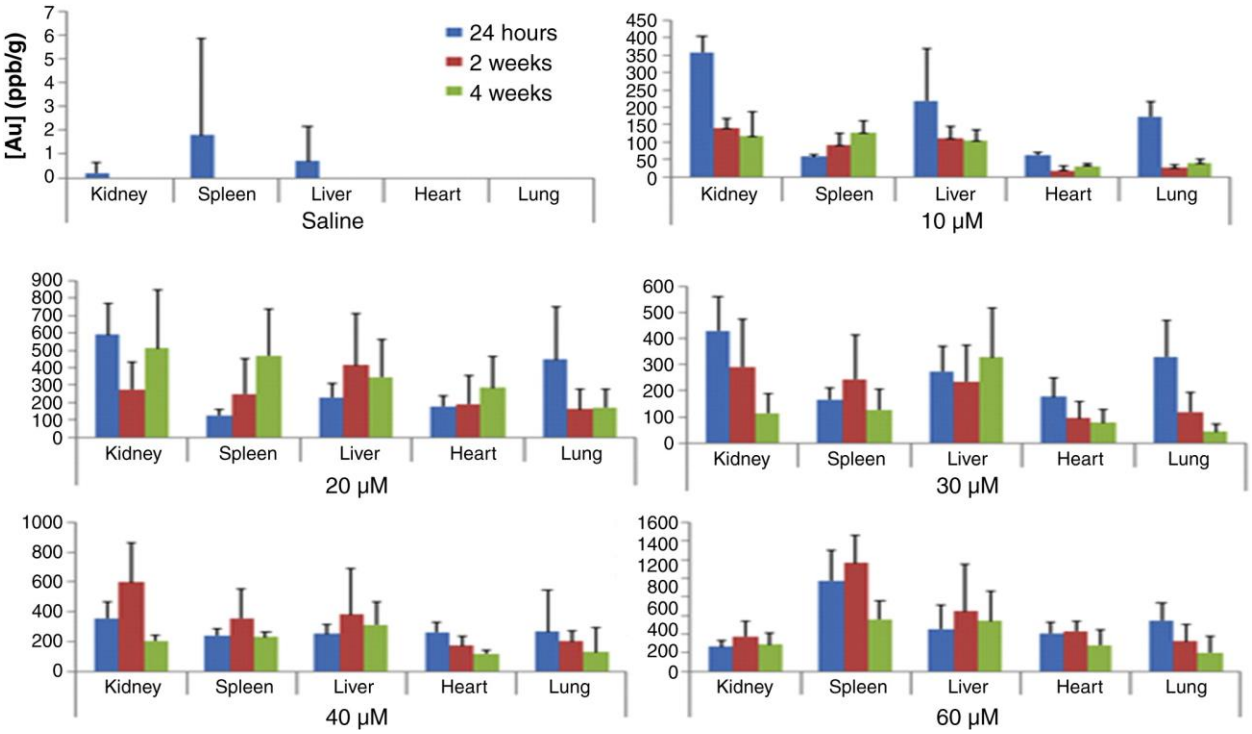

Figure 2. 12 Organ distribution analysis at 24 h, 2 weeks, and 4 weeks (n = 5 for each time point, 200 µL injections) show an initial accumulation within the kidney and lungs at 24 h. This accumulation shifts to the liver and spleen at 2 and 4-week time points, presumably because of RES clearance [46].

At low concentration, the injected Au nanoparticles tend to accumulate in the kidney, liver, and lung initially, but the particles' distribution shifts to the heart and spleen for higher injection concentration. As time went on, the accumulation shifts to liver and spleen for all injection concentration. Overall, glutathione-coated Au nanoparticles were greatly reduced in the heart and lung after 4 weeks but a small amount of the Au nanoparticles still remain in the liver and spleen as the injection concentration was increased. This shift is most likely due to the reticuloendothelial system clearance at higher injection concentration. In conclusion, the glutathione-coated Au nanoparticles show no toxicity at any concentration up to 60 μM, it also has the ability to target primary organs and gradually dissipated and cleared over time.

2.3 Galvanic Replacement Reaction

Galvanic replacement is an electrochemical reaction when two different metals are in electrical contact in an electrolyte; it consists of two half-reactions: metal with lower reduction potential will be corroded by the metal ions with higher reduction potential, in the meantime, the metal with higher potential will be reduced [47].

In our case, because Au (E^0 = 1.50 V vs. SHE) has higher reduction potential than Ag (E^0= 0.80 V vs. SHE) at room temperature, when AgNPs contact with aqueous chloroauric acid ($HAuCl_4$) solution, galvanic replacement will take place immediately at the site where has the highest surface energy on the AgNPs (step 1 in figure 2.13); Ag atoms will get corroded (oxide) by the $AuCl^-$ ions and release Ag^- ions into the solution and Au^{3+} ions will be reduced into Au atoms and deposited on the surface of the AgNPs [48], the reaction can be summarized as follow:

$$\text{Anode: } Ag_{(s)} \rightarrow Ag^{+}_{(aq)} + e^{-}_{(aq)} \quad (0.80 \text{ V vs. SHE}) \tag{2-1}$$

$$\text{Cathode: } Au^{3+}_{(aq)} + 3e^{-}_{(aq)} \rightarrow Au \quad (1.50 \text{ V vs. SHE}) \tag{2-2}$$

Combined reaction:

$$3Ag_{(s)} + AuCl_{4\,(aq)}^{-} \longrightarrow 3Ag_{(aq)}^{+} + Au_{(s)} + 4Cl_{(aq)}^{-} \quad (2\text{-}3)$$

this will result in creating small holes (step 2 in figure 2.13) on the surface of the nanoparticles since one Au^{3+} ion has to replace three Ag atoms in order to achieve charge balance (as shown in equation 2-3). As a result, the newly formed Au atoms will attach to the surface of the particles due to the both Au and Ag have same crystal structure (face-centered-cubic, fcc) and similar lattice constant (4.086 Å and 4.078 Å for Ag and Au, respectively). The deposition of Au atoms on the surface of the NPs will create a thin incomplete layer, which leads to small holes on the surface and continues to dissolve Ag atoms inside the particle (step 2 in figure 2.13). When the remaining Ag atoms are dissolved completely, the particle will transform into a pore-free, hollow Au-Ag nano-shells. If more $HAuCl_4$ solution is introduced at this point, the $AuCl^-$ ions will "dealloying" the Au-Ag nano-shells by selectively dissolving the Ag atom and cause the Au-Ag nano-shell break into much smaller pure AuNPs (step 5 in figure 2.13).

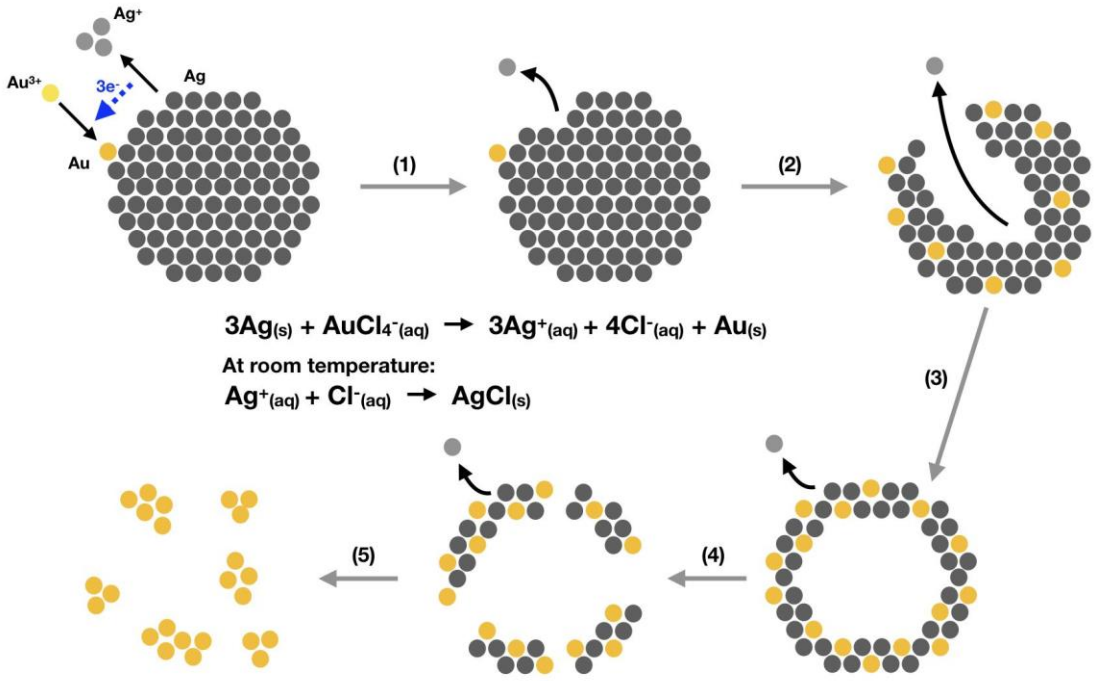

Figure 2. 13 Schematic illustration of the synthesis process of Au-AgNPs through galvanic replacement, grey dots and yellow dots represented Ag atoms and Au atoms respectively.

2.4 Electroless Deposition

The electroless deposition also refer to as electroless plating or autocatalytic plating, which is an electrochemical process that required no external power source. Unlike electrochemical deposition, electroless deposition has only one electrode and the electrolyte is more complex. It contains water, a reducing agent, and a metal salt. The setup is shown in figure 2.14.

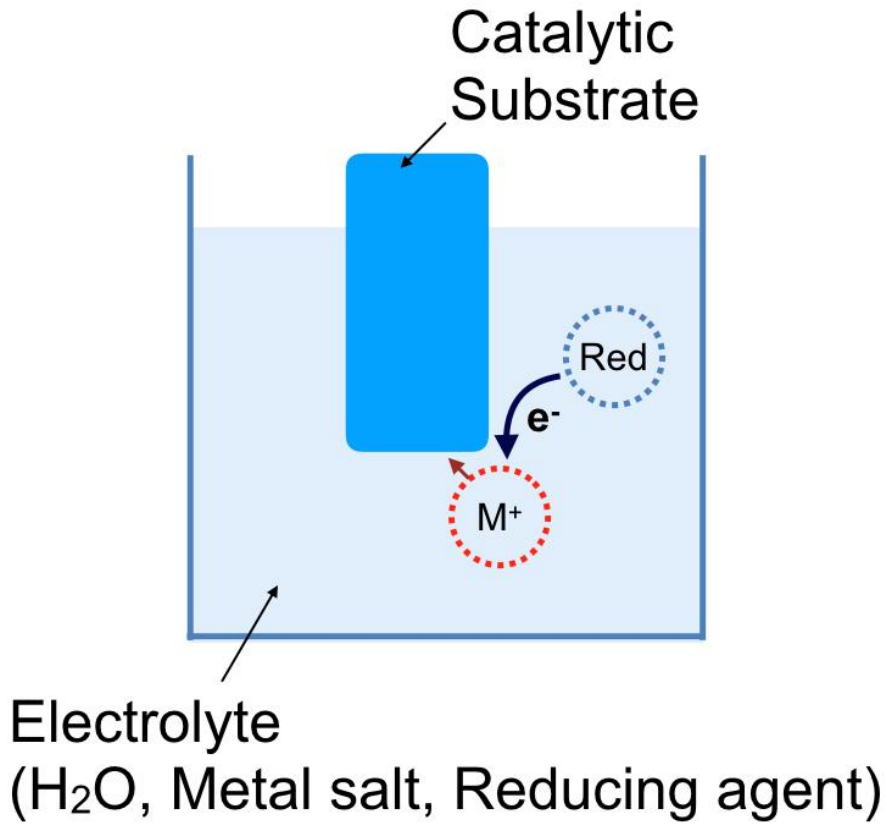

Figure 2. 14 The electrolytic cell for electroless deposition. Here M^+ and Red represented as metal ion and reducing agent, respectively.

During the electroless deposition process, the reducing agent in the electrolyte is the source of the electron; it donates electrons to the catalytic surface and releases hydrogen gas as the byproduct. The metal ion at the surface of the substrate obtain the electron and reduced on the surface. The reaction is presented as follow:

$$M^{z+}_{solutiom} + Red_{solution} \xrightarrow{\substack{Catalytic \\ Substrate}} M_{lattice} + Ox_{solution}$$

Where $Ox_{solution}$ represented as the oxidation of product of the reducing agent.

3. SYNTHESIS OF ULTRA-SMALL AU NANOPARTICLES BY GALVANIC REPLACEMENT REACTION OF LARGER AG NANOPARTICLES

In this section, the synthesis process and the characterization of the Au nanoparticles, the removal of the polyvinylpyrrolidone-coating, and the process of functionalization on the nanoparticle surface using glutathione were introduced.

3.1 Polyvinylpyrrolidone (PVP)-coated Au-Ag Nanoparticles

3.1.1 Synthesis of PVP coated Au-Ag NPs by Galvanic Replacement of Big Ag Nanoparticles

The synthesis process is as follows: To synthesis 2 mL of Ag-Au nanoparticles, 200 μL of 5 nm Ag nanoparticles solution (purchased from nanoComposix, Inc.) was diluted with 1800 μL of deionized water (Millipore), and then the desired amount of 0.01 M aqueous Au (III) chloride hydrate ($HAuCl_4 \bullet 3H_2O$, purchased from Sigma-Aldrich) solution was added with stirring. The replacement rate depends on the amount of $HAuCl_4$ added. The solution of 200 μL of 5 mg/mL 5 nm Ag nanoparticles contains about 9.27×10^{-6} mole of Ag atoms. To replace all the Ag atoms with Au, it needs about 3.09×10^{-6} mol of Au atoms since one Au atom can replace three Ag atoms. Thus, it required 309 μL of aqueous 0.01 M $HAuCl_4$ solution to completely replace all the Ag atoms in the solution and form pure Au nanoparticles theoretically. Table 3.1 shows the amount of $HAuCl_4$ solution that needs to be added to get a different replacement rate.

Table 3. 1 Different amount of $HAuCl_4$ solution required to achieve different replacement rate.

Replacement rate	AgNPs solution volume (μL)	$HAuCl_4$ solution volume (μL)
100%	2000	309
75%	2000	232
50%	2000	155
25%	2000	77

Silver nanoparticle solution was placed in a beaker with a magnetic stirrer stirring vigorously, the desired amount of 0.01 M aqueous $HAuCl_4 \cdot 3H_2O$ solution was added to Ag nanoparticle solution dropwise and let it react for 20 minutes. During the galvanic replacement, Ag^+ ions and Cl^- ions formed Ag chloride (AgCl) precipitate which usually has a much larger size. They can be easily removed by centrifuging the solution. AgCl particles will settle down at the bottom of the centrifuge tube, and Au/Au nanoparticles are too small to be settled down. After centrifuging the solution at 14,000 rpm for 20 minutes, the supernatant which contains Ag/Au small particles was transferred to a 3K (3,000 nominal molecular weight limit) Amicon Ultra-0.5 centrifugal filter device to wash away the remaining $HAuCl_4$ solution. In the end, 2 mL of deionized water was added back to the filter to re-suspend small particles.

3.1.2 Characterization of PVP-Coated Au-Ag Nanoparticles

Figure 3.3 shows the photograph of Au-Ag nanoparticles with the different replacement rate ranging from 0% (pure AgNPs) to 100% (pure AuNPs), it is obvious that the color of the samples change from yellow to purple when more Ag atoms are replaced by the Au atoms. UV-Vis absorption spectra (Figure 3.4) was obtained using PerkinElmer Lambda 35 UV/VIS Spectrometer. The UV-Vis sample was prepared by adding 50 μL of Au/Ag nanoparticle solution to 2 mL of deionized water. The result shows

that the absorption peak of those Ag-Au NPs shift from around 400 nm to 520 nm when the Ag nanoparticles are replaced with Au. It is interesting that there is a big gap between the 50% and 75% replacement rate, before the 50% replacement rate, the absorption peak lies around 410 nm; however, when the replacement rate reaches 75%, the absorption peak red-shifted to 505 nm. This is because before 50% of replacement rate, the particles are mostly made of Ag, once the replacement rate reaches more than 75%, there are more Au than Ag in the particles hence we can see this abrupt red-shift in the absorption spectrum.

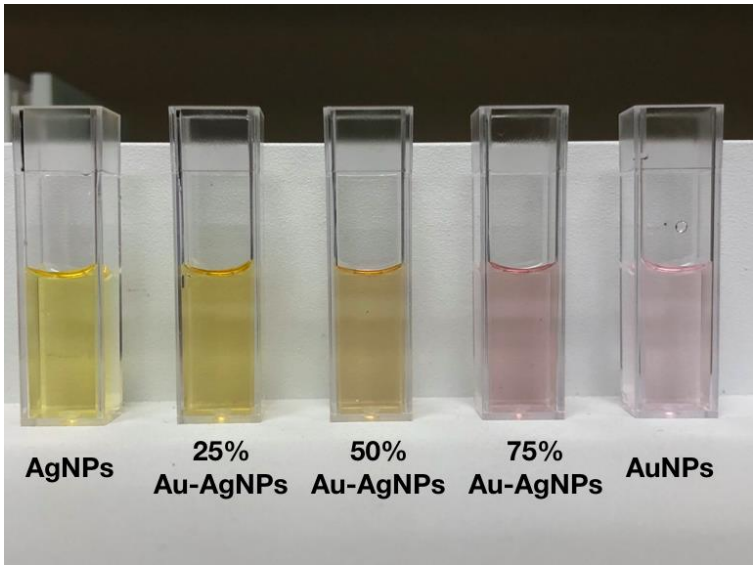

Figure 3. 1 Photograph of different replacement rate of diluted Ag-Au NPs solution from pure AgNPs (left) to pure AuNPs (right).

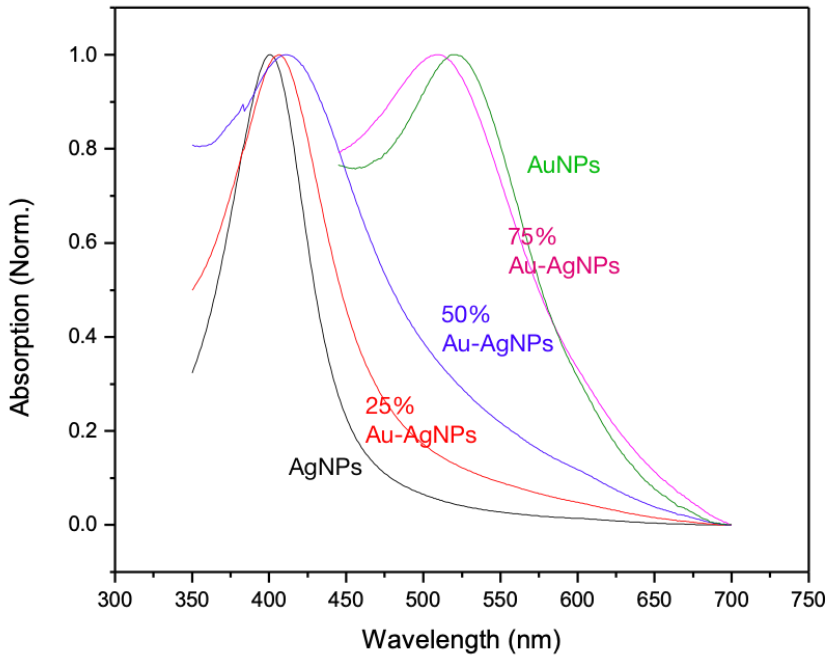

Figure 3. 2 Normalized UV-Vis absorption spectrum of Ag-Au NPs with the different replacement rates.

High-resolution transmission electron microscope (TEM) images of AgNPs and AuNPs were obtained (figure 3.5) in Hitachi H-9500 High-resolution TEM. Particle size distributions (figure 3.6 and figure 3.7) were measured using a imaging processing software. The TEM sample was prepared by dropping 10 µL of the particle solution onto a 3.0 mm Cu TEM grid. From the TEM images, it can be seen that the size difference between AgNPs and AuNPS. The AgNPs size are clearly much larger than AuNPs. The size distribution of the particles was calculated by measuring the individual nanoparticles' diameter from the TEM images by using ImageJ software. It can be seen that the particles size was greatly reduced from 6.65 nm to 2.53 nm after the replacement reaction. This is a clear evidence of the galvanic replacement since, as mentioned above, one Au atom can replace three Ag atoms in order to reach the charge balance.

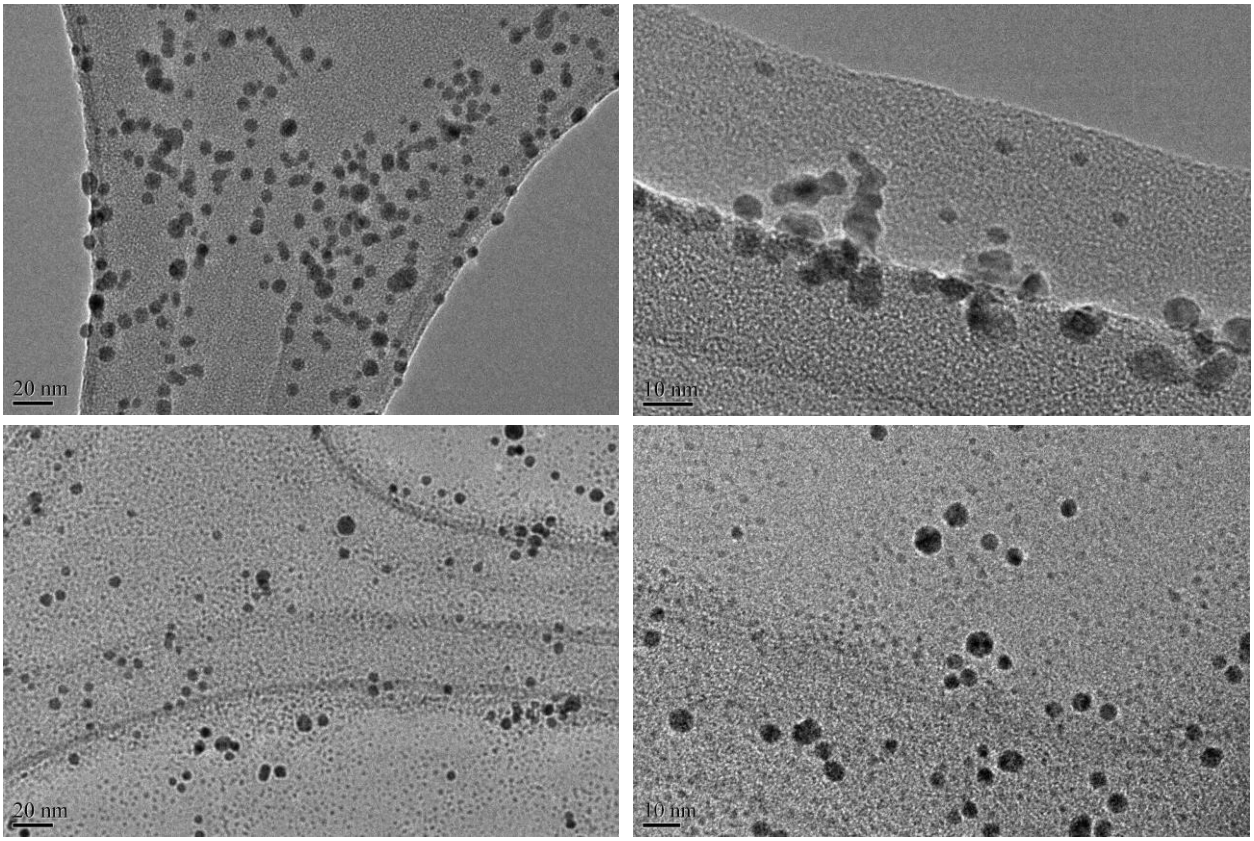

Figure 3. 3 TEM images of AgNPs (top) and AuNPs (bottom).

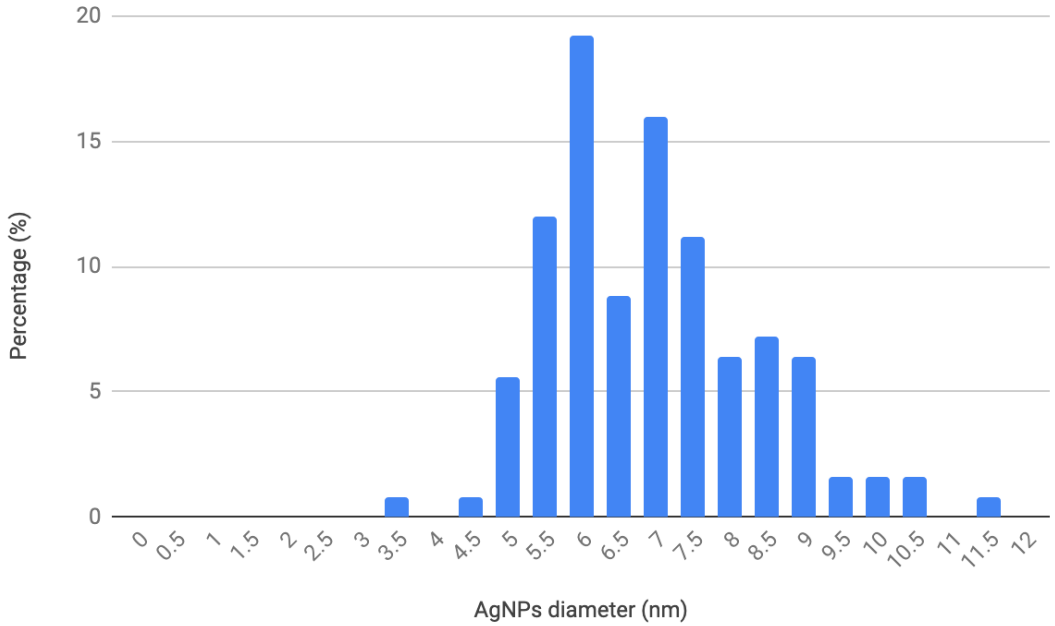

Figure 3. 4 Size distribution of AgNPs. The average diameter of AgNPs is 6.71 nm.

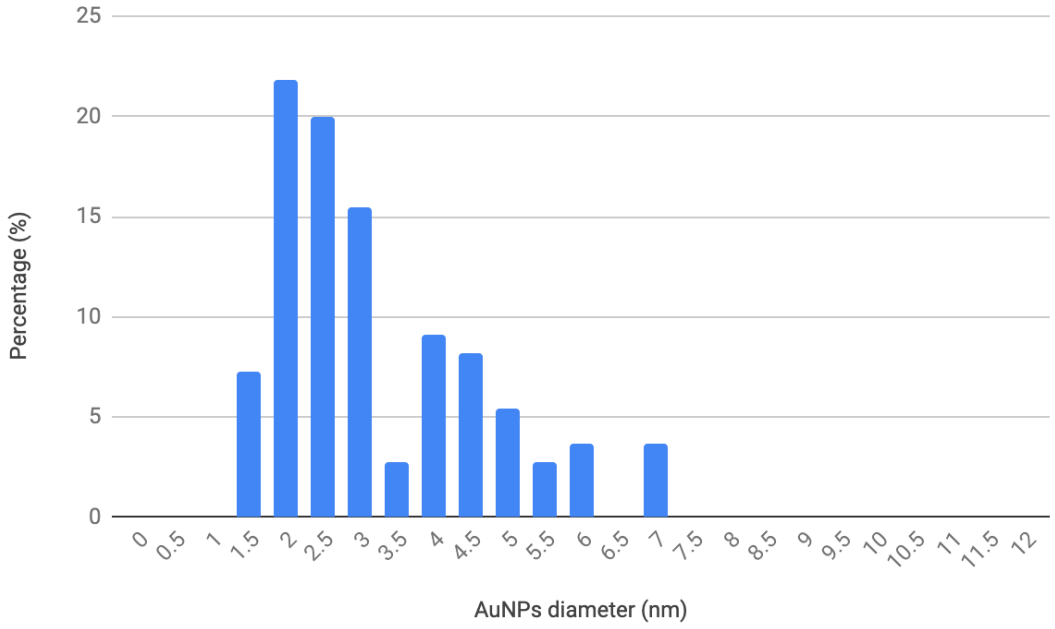

Figure 3. 5 Size distribution of AuNPs. The average diameter of AuNPs is 4.42 nm.

The inductively coupled plasma mass spectrometry (ICP-MS, Agilent 7500ce) was utilized to analyze the composition of the Au-Ag NPs with different replacement rate. The sample for ICP-MS was prepared as follows: 10 µL of Au-AgNPs was added to 90 µL of freshly made aqua regia, the mixture was diluted with 3% nitric acid to make the total volume to 2 mL. The results are shown in Table 3.2. The value of % Au is calculated by the concentration of Au divided by the amount of the Au atoms needed to replace all the Ag atoms, which is the concentration of Ag divided by three (since one Au atom have to replace three Ag atoms to reach the charge balance) plus the concentration of Au. This value gives us the experimental replacement rate of the Au-Ag NPs, which is very close to our theoretical replacement rate.

Table 3. 2 ICP-MS element analysis of Au-AgNPs with different replacement rate.

Sample Name	107 Ag (ppb)	197 Au (ppb)	% Au
Au-AgNPs (0%)	**3422.83**	**2.62**	**0.23**
Au-AgNPs (25%)	**2489.20**	**267.80**	**24.40**
Au-AgNPs (50%)	**1845.17**	**501.06**	**44.89**
Au-AgNPs (75%)	**1227.47**	**653.91**	**61.51**
Au-AgNPs (100%)	**145.88**	**849.26**	**94.58**

3.2 Naked AuNPs

3.2.1 Removing PVP Coating of Au Nanoparticles

AgNPs solution was mixed with acetone in the volume ratio of 1 (nanoparticle soulution):7 (Acetone), and then the mixed solution was centrifuged at 14,000 rpm for 20 min. After the centrifuge, the supernatant was removed and the precipitated AgNPs were transferred to a vacuum chamber to dry for 30 min to ensure the complete removal of acetone. Once the AgNPs were dried, deionized water was added to re-disperse the AgNPs. By adding $HAuCl_4$ solution to the AgNPs washed by using acetone, the galvanic replacement was initiated and the color changed from yellow to purple. After the reaction, the particles were centrifuged at 14,000 rpm for 20 min to remove the Ag chloride. The solution was transferred to a 3K Amicon Ultra-0.5 centrifugal filter device and centrifuged at 14,000 rpm for 15 min. After discarding the flow through, the deionized water was added back to the filter and centrifuge it again at 14,000 rpm for 15 min. This process was repeated three times to remove excess $HAuCl_4$ solution and remaining Ag chloride in the sample. After this washing process, the naked AuNPs were collected by simply reversing and placing the filter in a new collecting tube and centrifuge again to transfer the naked AuNPs from the filter to the collecting tube.

3.2.2 Characterization of Naked Au Nanoparticles

The magnitude of the zeta potential is a measure of the stability of a colloid system. The average zeta potential of PVP-coated AuNPs and naked AuNPs are found to be -11.12 ± 6.44 mV and -33.12 ± 1.81 mV, respectively, which indicates the removal of the PVP-coating. Since the naked AuNPs surface is positively charged, when it contacts with the water it can attract negatively charged ions to its surface, thus the zeta potential of naked AuNPs should be more negative than PVP-coated AuNPs.

3.3 AuNPs Smaller Than 2 nm

3.3.1 Isolation of AuNPs smaller than 2 nm

Since the synthesized AuNPs have a relatively large size distribution, ranging from 1.7 nm to 4 nm, to ensure a better renal clearance of AuNPs, we tried to isolate AuNPs with a diameter less than 2 nm from as-synthesized nanoparticles. We developed a simple and fast way to separate 2 nm AuNPs by using a 50K Amicon Ultra-0.5 centrifugal filter. For these filters, the nominal molecular weight limit (NMWL) tells the size of the pores inside the filter. The particle with weight larger than NMWL cannot pass through the filter membrane and stay inside the filter; on the other hands, particle smaller than NMWL can pass through the filter. We can use this NMWL to calculate the minimum diameter for naked AuNPs to stay inside the filter. Assuming that the AuNPs are perfectly spherical and the surface coating is removed completely with radius *r*, the volume of this naked spherical AuNPs is going to be

$$V = \frac{4}{3}\pi r^3 \quad (nm)$$

Since the density of metallic Au is 19.3×10^6 (g/m^3), the mass of a Au nanoparticle is

$$M = \frac{4}{3}\pi r^3 \times 19.3 \times 10^{-21} \quad (g)$$

Applied the atomic weight of Au (A.W. = 196.67 g/mol), we can get the number of the Au atom in a $2r$ nm AuNP, that is

$$MW_{AuNPs} = 6.02 \times 10^{23} \times 19.3 \times 10^6 \times \frac{4}{3}\pi r^3$$

For 50,000 NMWL filter, the maximum radius of AuNPs that can pass through the filter is:

$$\mathbf{50,000} = 6.02 \times 10^{23} \times 19.3 \times 10^{6} \times \frac{4}{3}\pi r^{3}$$

$$r = 1.009\, nm$$

Hence, for those smaller than 2.018 nm, it can pass through the filter.

The naked AuNPs solution was transferred to the 50K filter and centrifuged at 14,000 rpm for 10 min. The flow-through solution should contain naked AuNPs with a diameter less than 2nm.

3.3.2 Characterization of naked AuNPs smaller than 2 nm

The solution of naked AuNPs smaller than 2 nm appear to be colorless (shown in figure 3.9) since the AuNPs is too small to scatter light. The size and shape were determined by the TEM images (shown in figure 3.10). Compared to the unfiltered naked AuNPs (shown in figure 3.11), it is clear that 2 nm AuNPs is successfully separated from larger particles. The size distribution of AuNPs smaller than 2 nm is presented in figure 3.12, which shows that the average core size of these particles is 1.78 ± 0.36 nm. The energy-dispersive X-ray (EDX) spectrum was also been taken (shown in figure 3.13 and Table 3.4) and it confirmed that these ultra small nanoparticles are made of Au atoms.

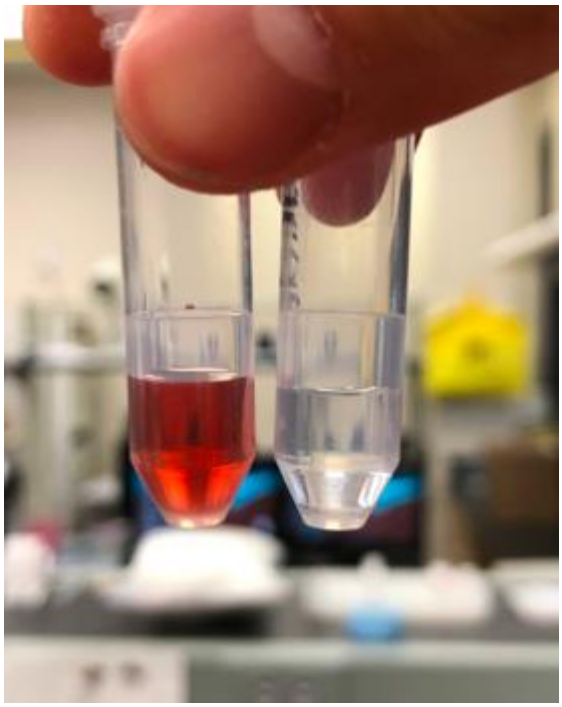

Figure 3. 6 The photograph of unfiltered AuNPs (left) and filtered 2 nm AuNPs.

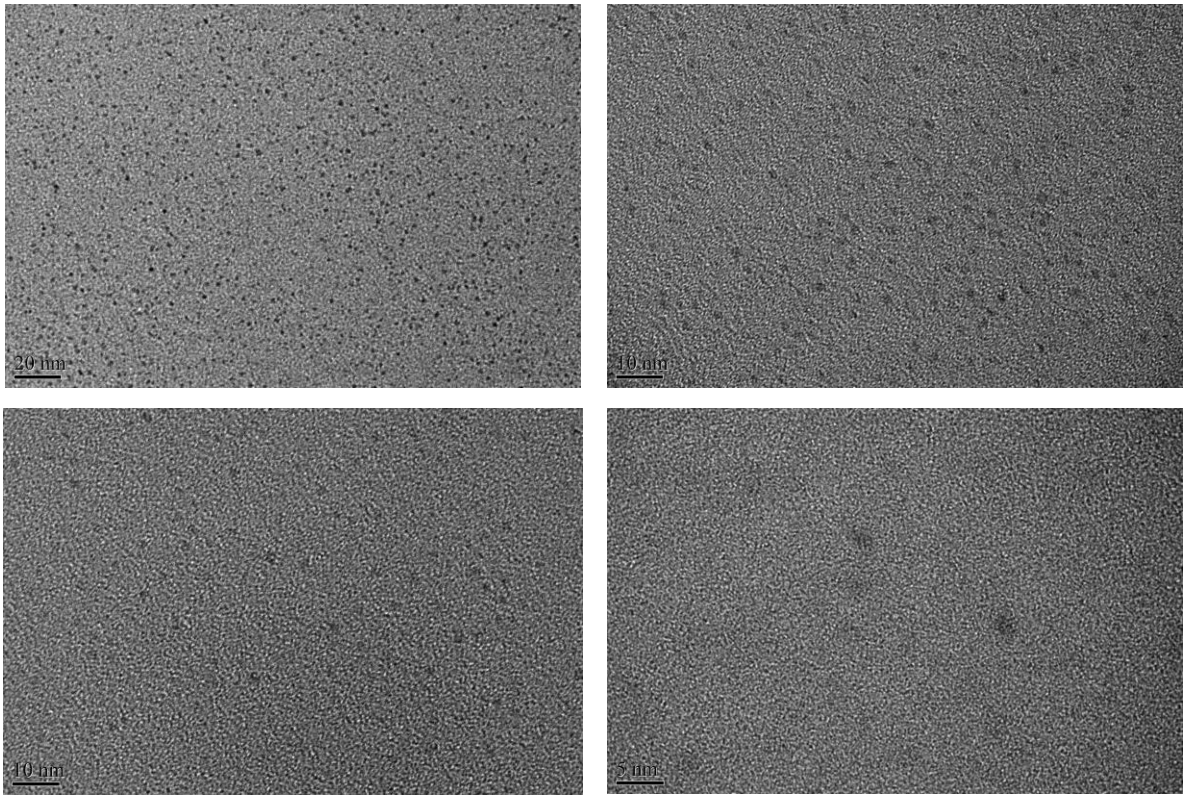

Figure 3. 7 TEM images of naked AuNPs smaller than 2 nm.

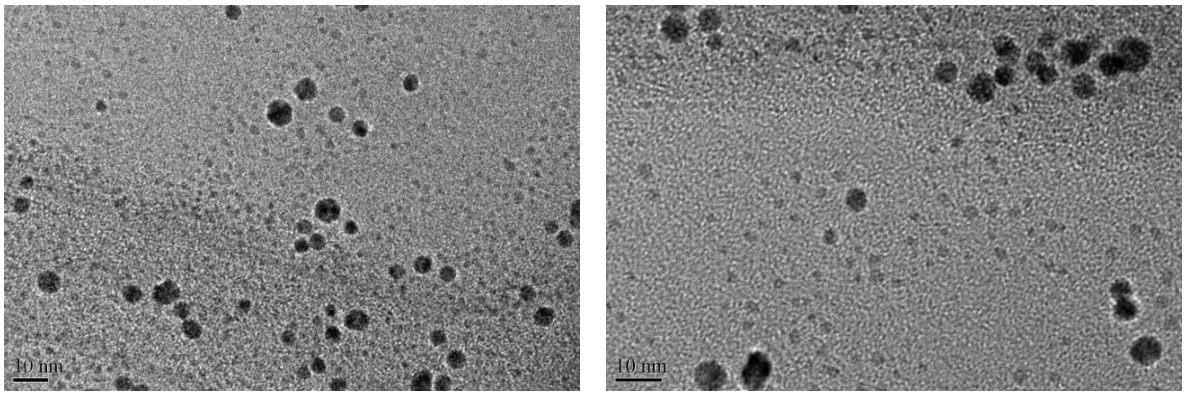

Figure 3. 8 TEM images of unfiltered naked AuNPs.

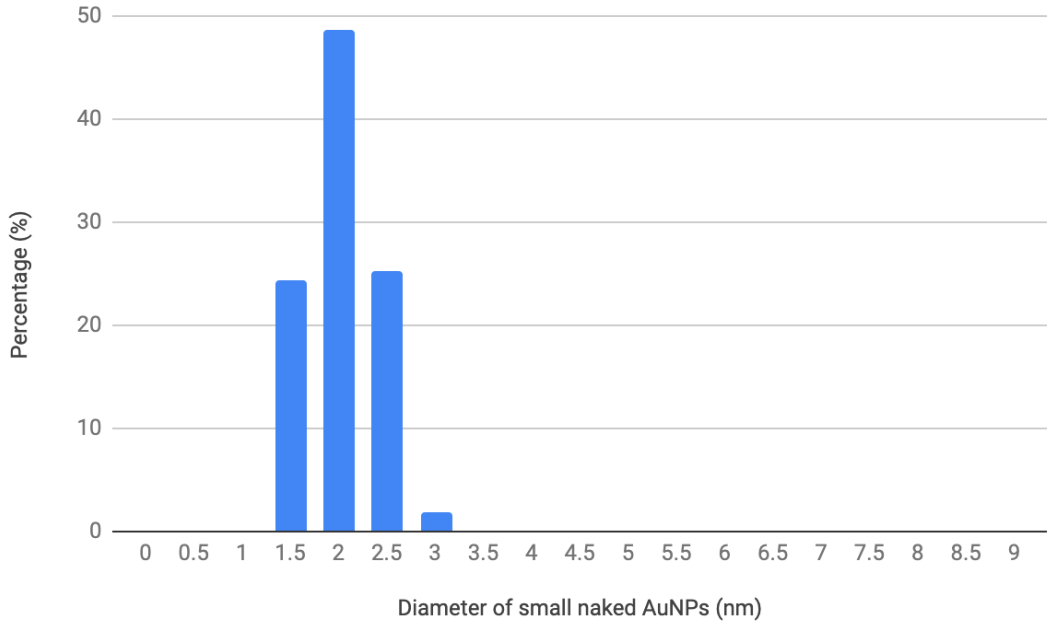

Figure 3. 9 Size distribution of ultra small naked AuNPs. The average diameter is 1.78 ± 0.36 nm.

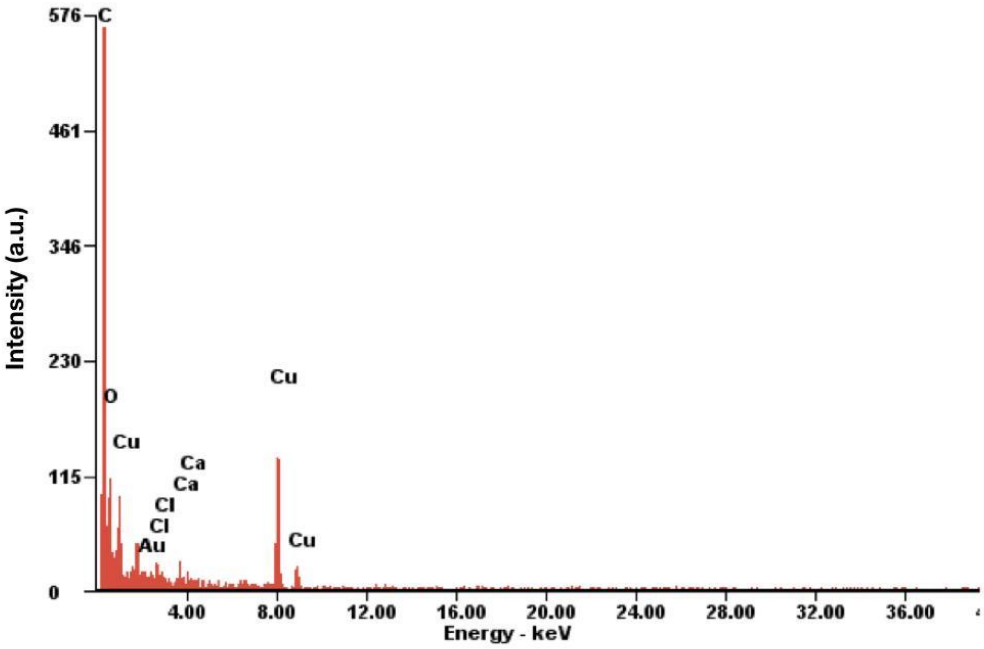

Figure 3. 10 EDX spectrum of ultra small naked AuNPs.

Table 3. 3 EDX element analysis of small naked AuNPs.

Element	Weight %	Atomic %
C K	76.10	90.00
O K	7.00	6.20
Au M	1.90	0.10
Cl K	0.70	0.30
Ca K	0.90	0.30
Cu K	13.5	3.00

3.4 Glutathione (GSH) -coated AuNPs

3.4.1 Synthesis

To synthesis GSH-coated AuNPs, 2 mL naked AgNPs solution was placed in a beaker with a magnetic stirrer. The mixture of 77.5 µL of 0.01 M aqueous GSH (L-glutathione reduced, purchased from Sigma-Aldrich) solution with 310 µL of 0.01 M aqueous $HAuCl_4$ solution is added to the naked AgNPs solution dropwise and stirred for a period of time. After the stirring process, the particles are centrifuged at 14,000 rpm for 20 min to remove Ag chloride particles. The solution was then transferred to a 3K Amicon Ultra-0.5 centrifugal filter and centrifuged at 14,000 rpm for 15 min. After discarding the flow-through solution, deionized water was added back to the filter and centrifuge it again at 14,000 rpm for 15 min. This process was repeated three times to remove excess $HAuCl_4$ solution and remaining Ag chloride in the sample. After this washing process, the GSH-coated AuNPs were collected by simply reversing the filter and placed in a new collecting tube and centrifuging to transfer the GSH-coated AuNPs from the filter to the collecting tube.

3.4.2 Characterization of GSH-coated AuNPs

The morphology and particle size distribution of GSH-coated AuNPs with different coating time are shown in figure 3.16, 3.17, and 3.18. As illustrated in figure 3.16, there is no observable difference between 30 min and 120 min of coating time, indicating that the coating time has no effect on the shape or cause aggregation of the particles. Serval additional TEM images were analyzed to quantify the size distribution and it was determined that the average size of the GSH-coated AuNPs with 30 min and 120 min are very similarly (4.52 ± 1.06 nm and 4.29 ± 1.04 nm, respectively) as shown in figure 3.17 and figure 3.18. The zeta potential of the particles was also measured and plotted as figure 3.19, it shows that at the first 60 minutes of the coating time, there is no significant change in zeta potential, however, after 60 minutes, the zeta potential increased drastically from -33.12 ± 1.81 mV to more than -16.06 ± 8.60 mV. The transition of the zeta potential indicates that the GSH is starting to coat onto the surface of the naked AuNPs.

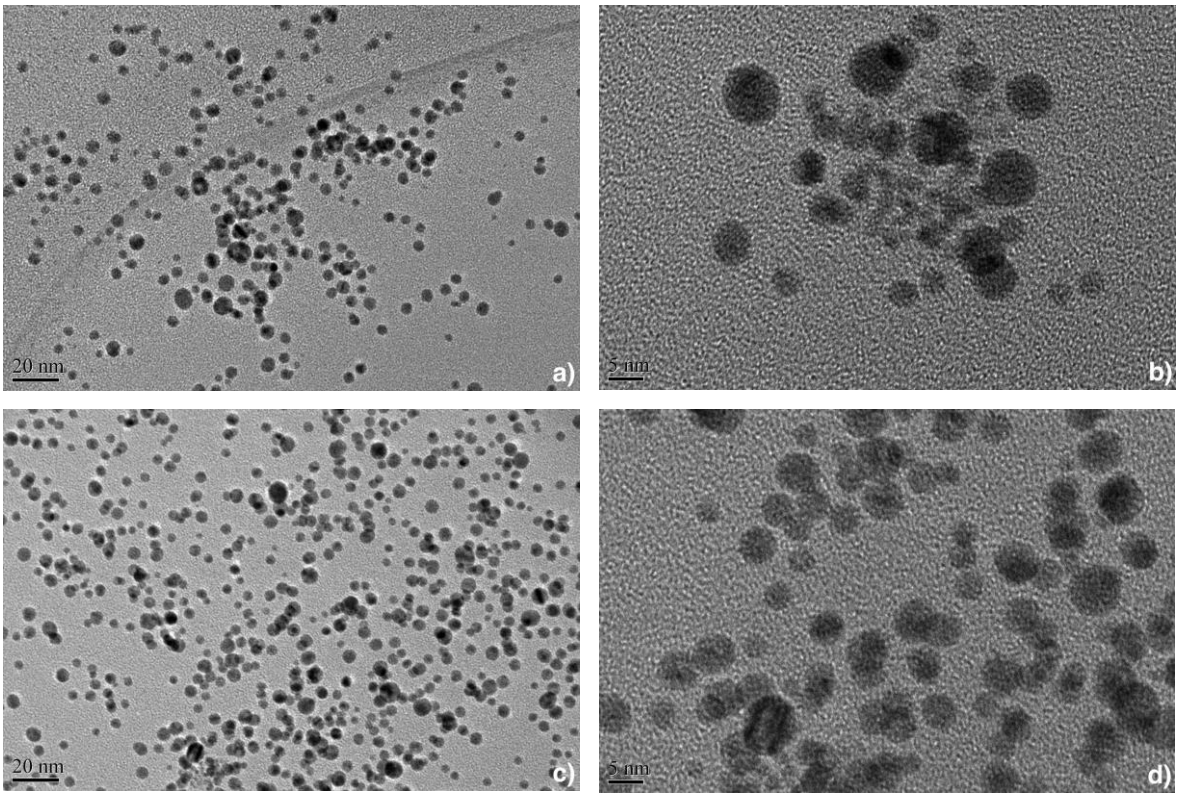

Figure 3. 11 TEM images of GSH-coated AuNPs with a) b) 30 min and c) d) 120 min of coating time.

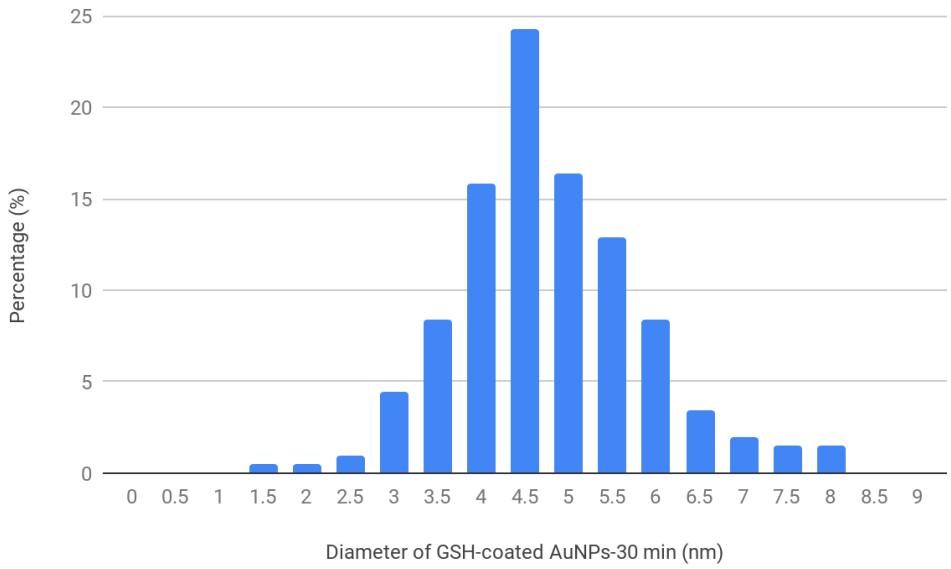

Figure 3. 12 The core size distribution of GSH-Coated AuNPs with 30 min of coating time. The average diameter is 4.52 ± 1.06 nm.

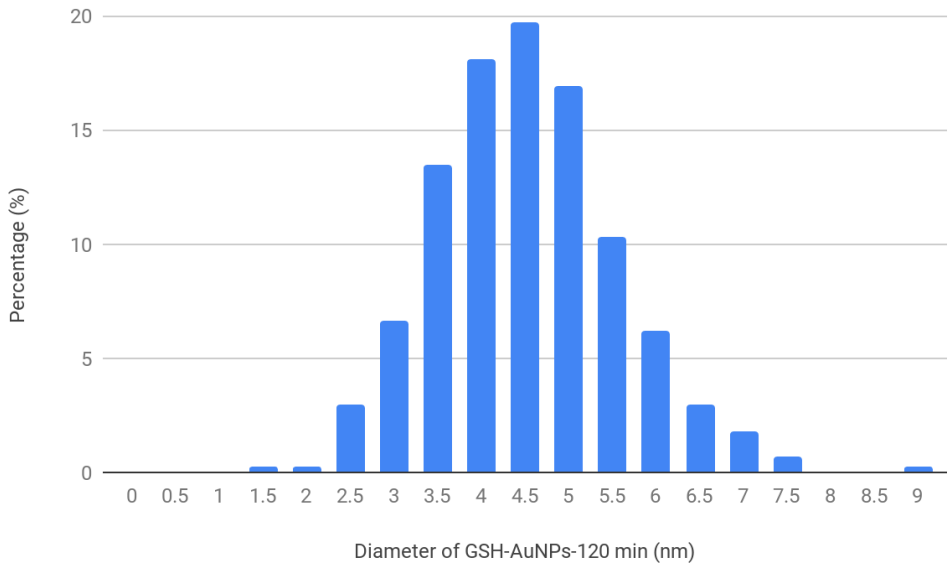

Figure 3. 13 The core size distribution of GSH-Coated AuNPs with 120 min of coating time. The average diameter is 4.29 ± 1.04 nm.

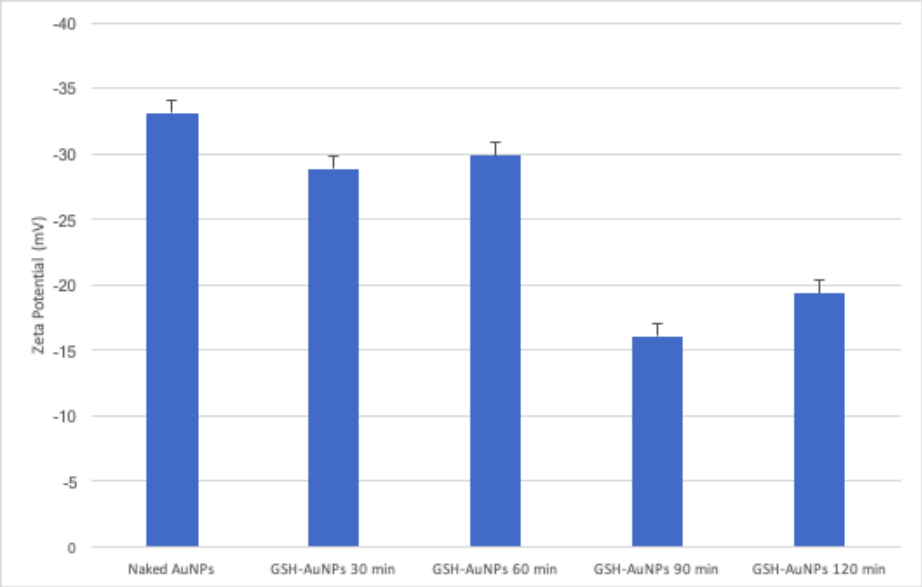

Figure 3. 14 The zeta potential of naked AuNPs, GSH-AuNPs 30 min, GSH-AuNPs 60 min, GSH-AuNPs 90 min, and GSH-AuNPs 120 min with an average potential of -33.12 ± 1.81 mV, -28.81 ± 6.04 mV, -29.83 ± 4.00 mV, -16.06 ± 8.60 mV, and -19.34 ± 4.39 mV respectively. All measurement was performed at room temperature.

4. INCORPORATION OF CU ONTO AU NANOPARTICLES BY ELECTROLESS DEPOSITION

We have developed an easy method to synthesize Au nanoparticles with a diameter less than 2 nm. Our ultimate goal is to use these renal clearable AuNPs as carriers to carry radioactive isotopes for clinical application. Our idea is to incorporate Cu isotope (^{64}Cu) on to the surface of our AuNPs since Cu-64 is a positron-emitting isotope and has been used in medical application such as molecular radiotherapy [49] and positron emission tomography [50]. To achieve this, we developed a process to deposit Cu onto the surface of AuNPs, which can be easily adopted for the incorporation of radioactive Cu.

4.1 Mechanism of Cu Electroless Deposition on AuNPs

The electrolytic cell used for this process is shown in figure 4.1:

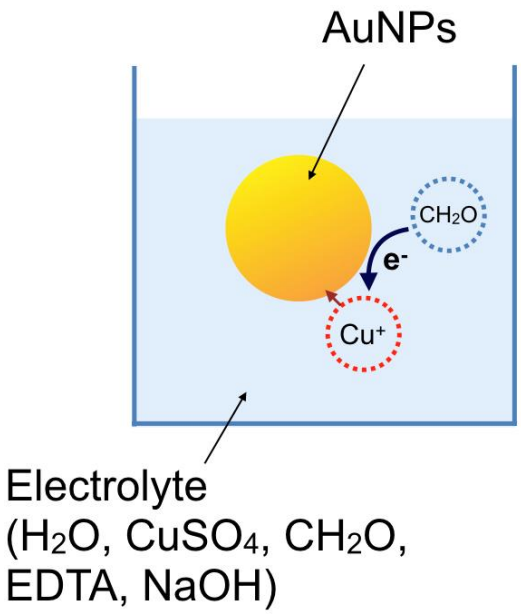

Figure 4. 1 The electrolytic cell of the Cu electroless deposition on AuNPs.

The AuNPs act as the catalytic surface and the formaldehyde (CH_2O) is the reducing agent. The Cu(II) sulfate ($CuSO_4$) is the metal salt which obtains the electron donated from formaldehyde near the surface of the AuNPs and forming Cu at the surface. The reaction is summarized as follows:

$$Anode: CH_2O + 3OH^- \rightarrow HCOO^- + 2H_2O + 2e^-$$

$$Cathode: Cu^{2+} + 2e^- \rightarrow Cu$$

Overall reaction:

$$Cu^{2+} + 2CH_2O + 4OH^- \xrightarrow{AuNPs} Cu + 2HCOO^- + 2H_2O + H_2$$

Notice that the electrolyte not only containing formaldehyde and Cu salt, it also contains Ethylenediaminetetraacetic acid (EDTA) and sodium hydroxide (NaOH). The reason why we add EDTA and NaOH in the electrolyte is that these two chemicals act as the complexing agent to prevent the formation of Cu in the solution instead of on the surface of AuNPs.

4.2 Electroless Deposition of Cu onto the Surface of the Au Nanoparticles (Cu-Au NPs)

To form Cu layer on the surface of the AuNPs, the Cu electroless electrolyte, which consists of 0.5 mL of 0.01 M Cu (II) sulfate pentahydrate ($CuSO_4 \cdot 5H_2O$) in 5% ethylenediaminetetraacetic acid (EDTA, Sigma-Aldrich), 0.5 mL of 1.0 M sodium hydroxide (NaOH, Am), and 0.5 mL of 37% formaldehyde (CH_2O, Sigma-Aldrich), is mixed with the AuNPs solution in volume ratio of 1:1 and let it react for 30 min to allow Cu to form on the surface of the AuNPs. After 30 min of mixing, the solution is transferred to a 30K Amicon filter and washed using deionized water to remove the excess, unreacted electrolyte.

4.3 Characterization of Cu-Au Nanoparticles (Cu-AuNPs)

When the Cu electroless electrolyte mixed with the AuNPs solution, the color of the solution changed from dark purple to orange (showed in figure 4.2). The TEM images (Figure 4.3) show that the diameter of the Cu-AuNPs is about 5 nm and the UV-Vis absorption spectrum (Figure 4.4) shows that the absorption peak of the Cu-AuNPs shift from 511 nm to 503 nm and it also has a secondary peak around 600 nm. To confirm the existence of Cu on the surface of the AuNPs, ICP-Ms was utilized and the results are shown in Table 4.1. By comparing the ICP-Ms element analysis results obtained from pure AuNPs and Cu-AuNPs, it can be seen that Cu-AuNPs does contain more Cu at 233 ppb than pure AuNPs at 0.7 ppb, indicating the existence of the Cu.

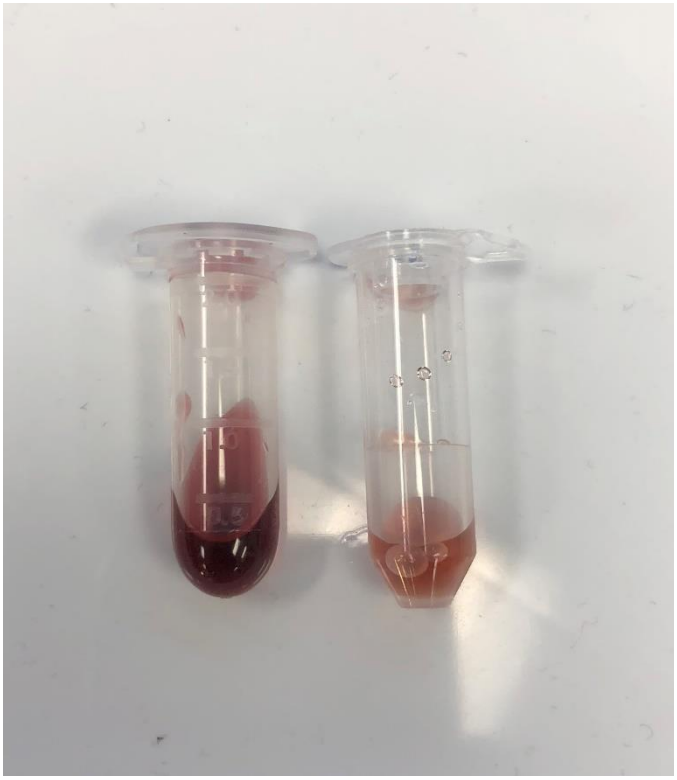

Figure 4. 2 Photographs of AuNPs (left) and Cu-AuNPs (right).

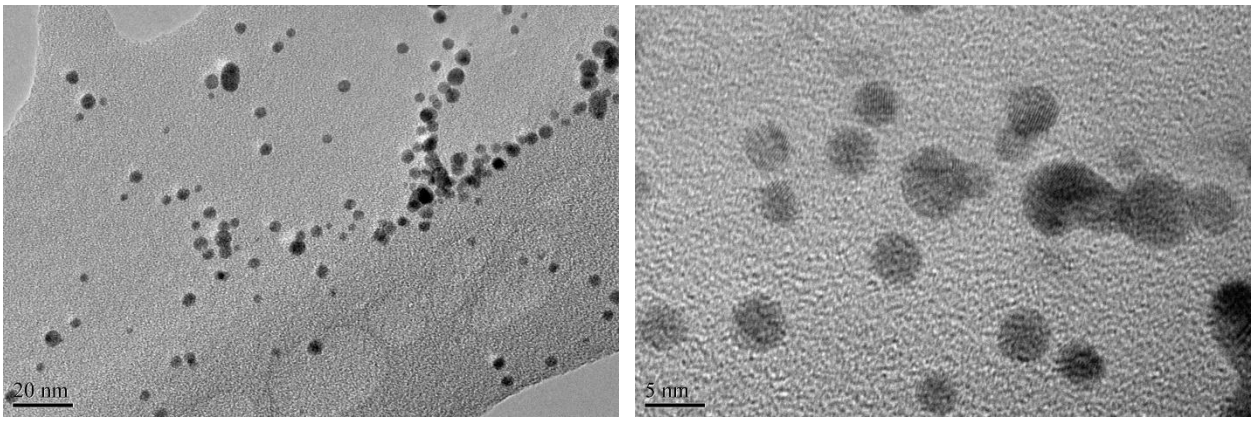

Figure 4. 3 TEM images of Cu-Au NPs. The average diameter of the Cu-AuNPs is about 4.3 nm.

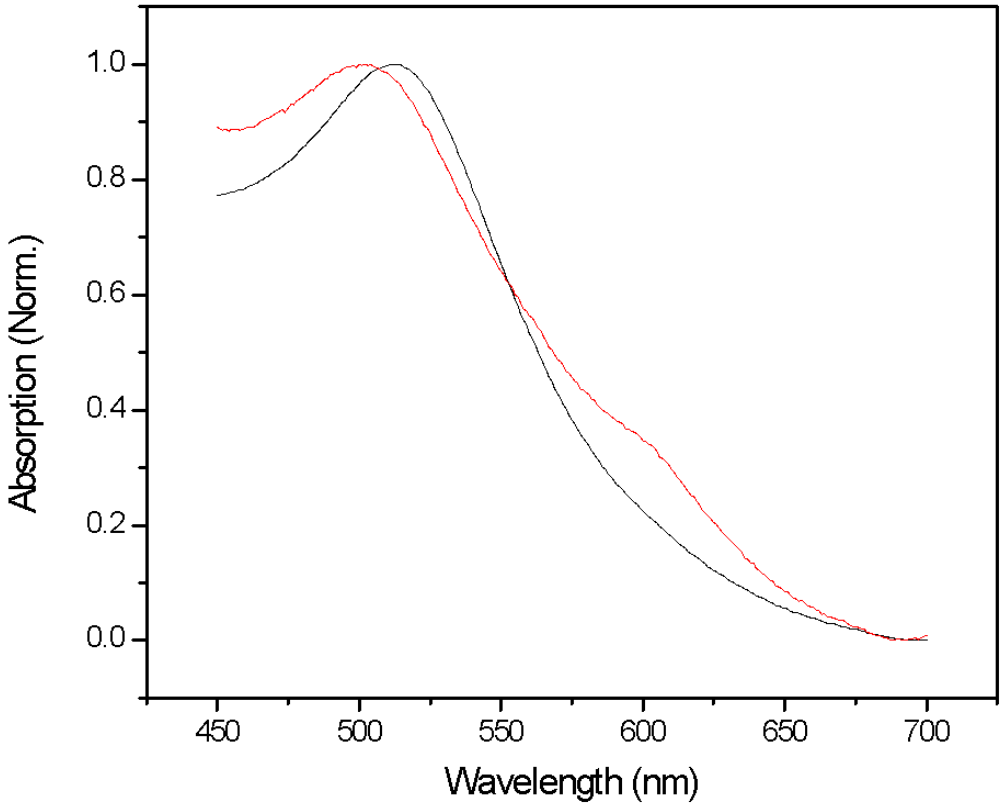

Figure 4. 4 UV-Vis absorption spectrua of AuNPs (black) and Cu-AuNPs (red).

Table 4. 1 ICP-MS elemental analysis result of AuNPs and Cu-AuNPs.

Sample Name	63 Cu [ppb]	63 Cu [M]	107 Ag [ppb]	107 Ag [M]	197 Au [ppb]	197 Au [M]
AuNPs	0.77	2.43×10^{-11}	89.73	1.66×10^{-9}	1044.39	1.06×10^{-8}
Cu-AuNPs	233.02	7.33×10^{-9}	53.71	9.96×10^{-10}	603.97	6.13×10^{-9}

4.4 Incorporation Rate of Cu onto the AuNPs

The incorporation rate of the Cu is studied furthermore. Two different concentrations of the electrolyte solution (0.01 M and 0.001 M) were used and the incorporation rate of the Cu was recorded in the different time interval. ICP-MS was utilized to analyze the result.

For 0.01 M of Cu electroless electrolyte, the ICP-MS element analysis result is presented in table 4.2 and figure 4.5. From figure 4.5, the incorporation rate of Cu increases with the first two hours, however, when the time reached 5 hours, the incorporation rate drops to 15.5% and continue to decrease to 5.7% after 8 hours of reaction time.

Table 4. 2 ICP-MS element analysis of 0.01 M electrolyte Cu-AuNPs.

Time (hour)	63 Cu (ppb)	107 Ag (ppb)	197 Au (ppb)	Incorporation Rate (%)
1 hr	182.9	28.5	112.7	35.4
2 hr	381.8	54.9	242.4	73.9
5 hr	79.9	34.7	98.6	15.5
8hr	29.4	57.7	223.9	5.7

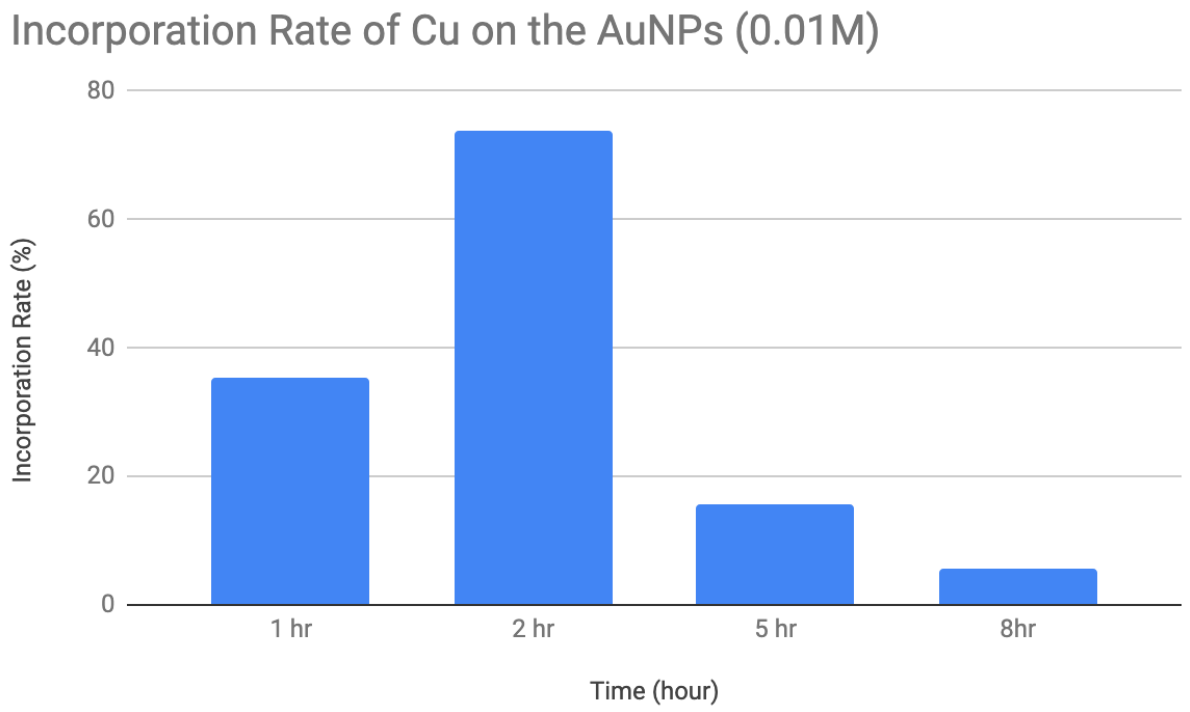

Figure 4. 5 The incorporation rate of Cu-AuNPs with 0.01 M of Cu electroless electrolyte.

Then we tried to decrease the concentration of the electrolyte and tested whether or not it can have better incorporation rate. The concentration was decreased to 0.001 M and the IC-MS element analysis is shown in table 4.3 and figure 4.6.

Table 4. 3 ICP-MS element analysis of 0.001 M electrolyte Cu-AuNPs.

Time (hour)	63 Cu (ppb)	107 Ag (ppb)	197 Au (ppb)	Incorporation Rate (%)
1 hr	13.4	35.6	177	23.5
2 hr	24.3	32.6	151	42.6
5 hr	5.3	39.9	185.3	9.2
8hr	4.5	36.8	145	7.9

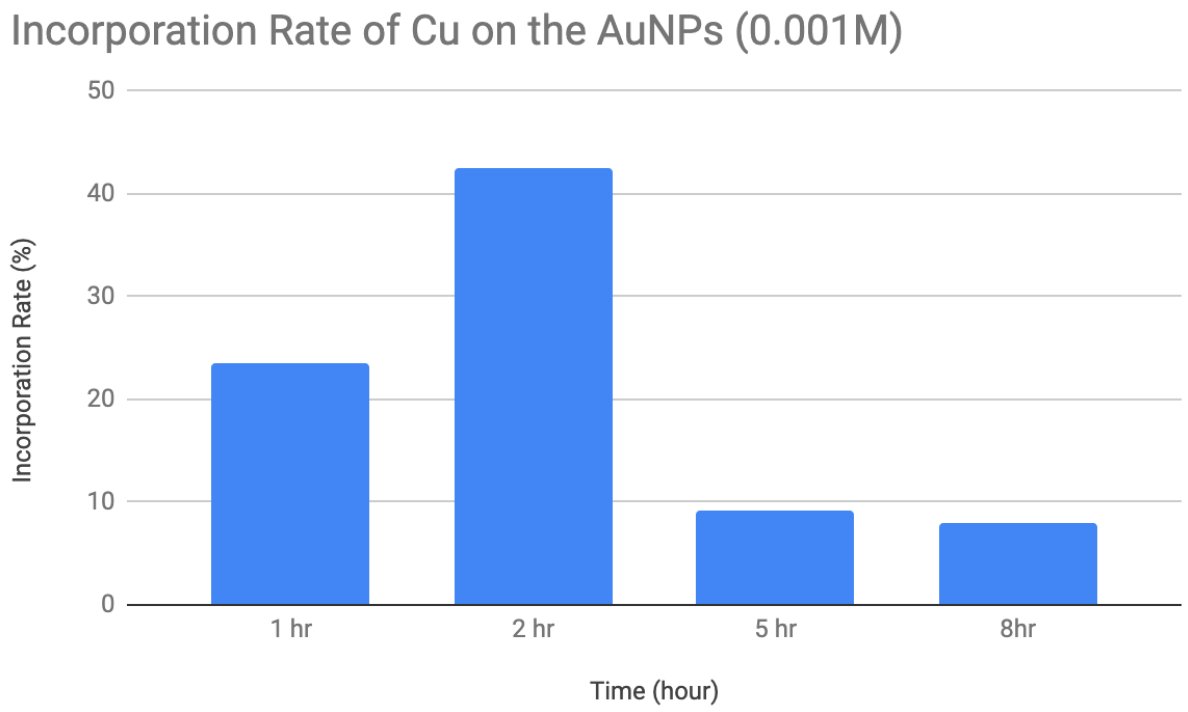

Figure 4. 6 The incorporation rate of Cu-AuNPs with 0.001 M of Cu electroless electrolyte.

Decreasing the concentration of the Cu electroless deposition electrolyte did not help the incorporation rate at all. We see the same thing again: the incorporation rate increase in the first two hours, but the incorporation rate drops to less than 10% after 5 hours and continue to decrease after that. This result indicated that the incorporated Cu is not very stable for our small AuNPs. The incorporated Cu can stay on AuNPs for short period of time, then it started to leach out when the time went on. This would be problematic since we need Cu to stay with AuNPs when it is used as the imaging agent or other in vivo applications.

5. CONCLUSION

Glutathione-coated Au nanoparticles with size less than 2 nm have been synthesized. These renal clearable nanoparticles have a promising potential to be used as carrier carrying radioactive isotopes such as Cu-64 for cancer imaging and treatments.

An easy and fast way to synthesize ultra small Au nanoparticles with an average diameter less than 5 nm has been developed, simply using galvanic replacement reaction to replace spherical Ag nanoparticles with Au chloroaurate. This synthesis process can be completed within an hour at room temperature.

Since the renal clearance of the nanoparticles are also strongly related to the surface chemistry of the nanoparticles, and the Ag nanoparticles we used for the synthesis of Au nanoparticles have polyvinylpyrrolidone (PVP) coating on the surface which is not an ideal surface coating for renal clearance, a simple way to remove the PVP coating by washing the particles with acetone has been developed. The optimum conditions have been found to functionalize Au nanoparticles with glutathione which is an excellent surface coating choice for renal clearance.

Also, we have developed a process to incorporate Cu on to the surface of these Au nanoparticles using the electroless deposition process. However, it has been found that incorporated Cu is not stable, leaching out inside a water suspension. Seeking another way to attach Cu to our Au nanoparticles is demanded.

LIST OF REFERENCE

[1] National Nanotechnology Initiative; U.S. National Nanotechnology Initiative: Washington, DC. www.nano.gov (accessed March 2015).

[2] Roco, Mihail C. "The long view of nanotechnology development: the National Nanotechnology Initiative at 10 years." (2011): 427-445.

[3] Dreaden, Erik C., Alaaldin M. Alkilany, Xiaohua Huang, Catherine J. Murphy, and Mostafa A. El-Sayed. "The golden age: gold nanoparticles for biomedicine." *Chemical Society Reviews* 41, no. 7 (2012): 2740-2779.

[4] Jain, Prashant K., Kyeong Seok Lee, Ivan H. El-Sayed, and Mostafa A. El-Sayed. "Calculated absorption and scattering properties of gold nanoparticles of different size, shape, and composition: applications in biological imaging and biomedicine." *The journal of physical chemistry B*110, no. 14 (2006): 7238-7248.

[5] Zeng, Shuwen, Ken-Tye Yong, Indrajit Roy, Xuan-Quyen Dinh, Xia Yu, and Feng Luan. "A review on functionalized gold nanoparticles for biosensing applications." *Plasmonics* 6, no. 3 (2011): 491.

[6] Saha, Krishnendu, Sarit S. Agasti, Chaekyu Kim, Xiaoning Li, and Vincent M. Rotello. "Gold nanoparticles in chemical and biological sensing." *Chemical reviews* 112, no. 5 (2012): 2739-2779.

[7] Hainfeld, J. F., D. N. Slatkin, T. M. Focella, and H. M. Smilowitz. "Gold nanoparticles: a new X-ray contrast agent." *The British journal of radiology* 79, no. 939 (2006): 248-253.

[8] Copland, John A., Mohammad Eghtedari, Vsevolod L. Popov, Nicholas Kotov, Natasha Mamedova, Massoud Motamedi, and Alexander A. Oraevsky. "Bioconjugated gold nanoparticles as a molecular based contrast agent: implications for imaging of deep tumors using optoacoustic tomography." *Molecular Imaging & Biology* 6, no. 5 (2004): 341-349.

[9] Simpson, Carrie A., Kenneth J. Salleng, David E. Cliffel, and Daniel L. Feldheim. "In vivo toxicity, biodistribution, and clearance of glutathione-coated gold nanoparticles." *Nanomedicine: Nanotechnology, Biology and Medicine* 9, no. 2 (2013): 257-263.

[10] Freestone, Ian, Nigel Meeks, Margaret Sax, and Catherine Higgitt. "The Lycurgus cup—a roman nanotechnology." *Gold bulletin* 40, no. 4 (2007): 270-277.

[11] Faraday M (January 1857). "The Bakerian Lecture: Experimental Relations of Gold (and Other Metals) to Light". Philosophical Transactions of the Royal Society of London. 147: 145–181.

[12] Freestone, Ian, Nigel Meeks, Margaret Sax, and Catherine Higgitt. "The Lycurgus cup—a roman nanotechnology." *Gold bulletin* 40, no. 4 (2007): 270-277.

[13] Turkevitch, J. "Colloidal gold. Part I: historical and preparative aspects, morphology and structure." Gold Bulletin 91 (1886).

[14] Martin, Charles R. "Nanomaterials: a membrane-based synthetic approach." *Science* 266, no. 5193 (1994): 1961-1966.

[15] Kim, Franklin, Jae Hee Song, and Peidong Yang. "Photochemical synthesis of gold nanorods." *Journal of the American Chemical Society* 124, no. 48 (2002): 14316-14317.

[16] Jana, Nikhil R., Latha Gearheart, and Catherine J. Murphy. "Seed-mediated growth approach for shape-controlled synthesis of spheroidal and rod-like gold nanoparticles using a surfactant template." *Advanced Materials* 13, no. 18 (2001): 1389-1393.

[17] Gans R (1912) The shape of ultra microscopic gold particles. *Ann. Phys.* (37):881

[18] Skrabalak, Sara E., Jingyi Chen, Yugang Sun, Xianmao Lu, Leslie Au, Claire M. Cobley, and Younan Xia. "Gold nanocages: synthesis, properties, and applications." Accounts of chemical research 41, no. 12 (2008): 1587-1595.

[19] Oldenburg, S. J., R. D. Averitt, S. L. Westcott, and N. J. Halas. "Nanoengineering of optical resonances." Chemical Physics Letters 288, no. 2-4 (1998): 243-247.

[20] Turkevitch, J. "Colloidal gold. Part I: historical and preparative aspects, morphology and structure." Gold Bulletin 91 (1886).

[21] Brust, Mathias, Merryl Walker, Donald Bethell, David J. Schiffrin, and Robin Whyman. "Synthesis of thiol-derivatised gold nanoparticles in a two-phase liquid–liquid system." Journal of the Chemical Society, Chemical Communications 7 (1994): 801-802.

[22] Lohse, Samuel E., and Catherine J. Murphy. "The quest for shape control: a history of gold nanorod synthesis." Chemistry of Materials 25, no. 8 (2013): 1250-1261.

[23] Indrasekara, A. Swarnapali DS, Robert C. Wadams, and Laura Fabris. "Ligand exchange on gold nanorods: going back to the future." Particle & Particle Systems Characterization 31, no. 8 (2014): 819-838.

[24] Yu, Yu-Ying, Ser-Sing Chang, Chien-Liang Lee, and CR Chris Wang. "Gold nanorods: electrochemical synthesis and optical properties." The Journal of Physical Chemistry B 101, no. 34 (1997): 6661-6664.

[25] Jana, Nikhil R., Latha Gearheart, and Catherine J. Murphy. "Seed-mediated growth approach for shape-controlled synthesis of spheroidal and rod-like gold nanoparticles using a surfactant template." Advanced Materials 13, no. 18 (2001): 1389-1393.

[26] Skrabalak, Sara E., Jingyi Chen, Yugang Sun, Xianmao Lu, Leslie Au, Claire M. Cobley, and Younan Xia. "Gold nanocages: synthesis, properties, and applications." Accounts of chemical research 41, no. 12 (2008): 1587-1595.

[27] Oldenburg, S. J., R. D. Averitt, S. L. Westcott, and N. J. Halas. "Nanoengineering of optical resonances." Chemical Physics Letters 288, no. 2-4 (1998): 243-247.

[28] Xin, Wenbo, Joseph Severino, Igor M. De Rosa, Dian Yu, Jeffrey Mckay, Peiyi Ye, Xunqian Yin, Jenn-Ming Yang, Larry Carlson, and Suneel Kodambaka. "One-step synthesis of tunable-size gold nanoplates on graphene multilayers." Nano letters 18, no. 3 (2018): 1875-1881.

[29] Shang, Li, Shaojun Dong, and G. Ulrich Nienhaus. "Ultra-small fluorescent metal nanoclusters: synthesis and biological applications." Nano today 6, no. 4 (2011): 401-418.

[30] Cui, Malin, Yuan Zhao, and Qijun Song. "Synthesis, optical properties and applications of ultra-small luminescent gold nanoclusters." TrAC Trends in Analytical Chemistry 57 (2014): 73-82.

[31] Zhu, Manzhou, Christine M. Aikens, Frederick J. Hollander, George C. Schatz, and Rongchao Jin. "Correlating the crystal structure of a thiol-protected Au25 cluster and optical properties." Journal of the American Chemical Society 130, no. 18 (2008): 5883-5885.

[32] Negishi, Yuichi, Katsuyuki Nobusada, and Tatsuya Tsukuda. "Glutathione-protected gold clusters revisited: Bridging the gap between gold (I)− thiolate complexes and thiolate-protected gold nanocrystals." Journal of the American Chemical Society 127, no. 14 (2005): 5261-5270.

[33] Yue, Yuan, Tian-Ying Liu, Hong-Wei Li, Zhongying Liu, and Yuqing Wu. "Microwave-assisted synthesis of BSA-protected small gold nanoclusters and their fluorescence-enhanced sensing of silver (I) ions." Nanoscale 4, no. 7 (2012): 2251-2254.

[34] Choi, Hak Soo, Wenhao Liu, Preeti Misra, Eiichi Tanaka, John P. Zimmer, Binil Itty Ipe, Moungi G. Bawendi, and John V. Frangioni. "Renal clearance of quantum dots." Nature biotechnology 25, no. 10 (2007): 1165.

[35] Ganong, William Francis, and Kim E. Barrett. Ganong's review of medical physiology. McGraw-Hill Medical, 2012.

[36] Liu, Jinbin, Mengxiao Yu, Chen Zhou, and Jie Zheng. "Renal clearable inorganic nanoparticles: a new frontier of bionanotechnology." Materials Today 16, no. 12 (2013): 477-486.

[37] Ohlson, Maria, Jenny Sorensson, and Borje Haraldsson. "A gel-membrane model of glomerular charge and size selectivity in series." American Journal of Physiology-Renal Physiology 280, no. 3 (2001): F396-F405.

[38] Kumar, Ashutosh, Alok K. Pandey, Shashi S. Singh, Rishi Shanker, and Alok Dhawan. "Cellular uptake and mutagenic potential of metal oxide nanoparticles in bacterial cells." Chemosphere 83, no. 8 (2011): 1124-1132.

[39] Feng, Qiyi, Yanping Liu, Jian Huang, Ke Chen, Jinxing Huang, and Kai Xiao. "Uptake, distribution, clearance, and toxicity of iron oxide nanoparticles with different sizes and coatings." Scientific reports 8, no. 1 (2018): 2082

[40] Bayliss, Sue C., Robert Heald, D. Ian Fletcher, and Lorraine D. Buckberry. "The culture of mammalian cells on nanostructured silicon." Advanced Materials 11, no. 4 (1999): 318-321.

[41] Canham, Leigh T. "Bioactive silicon structure fabrication through nanoetching techniques." Advanced Materials 7, no. 12 (1995): 1033-1037.

[42] Popplewell, J. F., S. J. King, J. P. Day, P. Ackrill, L. K. Fifield, R. G. Cresswell, M. L. Di Tada, and Kexin Liu. "Kinetics of uptake and elimination of silicic acid by a human subject: a novel application of 32Si and accelerator mass spectrometry." *Journal of Inorganic Biochemistry* 69, no. 3 (1998): 177-180.

[43] Park, Ji-Ho, Luo Gu, Geoffrey Von Maltzahn, Erkki Ruoslahti, Sangeeta N. Bhatia, and Michael J. Sailor. "Biodegradable luminescent porous silicon nanoparticles for in vivo applications." Nature materials 8, no. 4 (2009): 331.

[44] Ghosh, Partha, Gang Han, Mrinmoy De, Chae Kyu Kim, and Vincent M. Rotello. "Gold nanoparticles in delivery applications." Advanced drug delivery reviews 60, no. 11 (2008): 1307-1315.

[45] Tiwari, Pooja, Komal Vig, Vida Dennis, and Shree Singh. "Functionalized gold nanoparticles and their biomedical applications." Nanomaterials 1, no. 1 (2011): 31-63.

[46] Simpson, Carrie A., Kenneth J. Salleng, David E. Cliffel, and Daniel L. Feldheim. "In vivo toxicity, biodistribution, and clearance of glutathione-coated gold nanoparticles." Nanomedicine: Nanotechnology, Biology and Medicine 9, no. 2 (2013): 257-263.

[47] Simpson, Carrie A., Kenneth J. Salleng, David E. Cliffel, and Daniel L. Feldheim. "In vivo toxicity, biodistribution, and clearance of glutathione-coated gold nanoparticles." Nanomedicine: Nanotechnology, Biology and Medicine 9, no. 2 (2013): 257-263.

[48] Hong, Xun, Dingsheng Wang, Shuangfei Cai, Hongpan Rong, and Yadong Li. "Single-crystalline octahedral Au–Ag nanoframes." Journal of the American Chemical Society 134, no. 44 (2012): 18165-18168.

[49] Anderson, Carolyn J., Lynne A. Jones, Laura A. Bass, Elizabeth LC Sherman, Deborah W. McCarthy, P. Duffy Cutler, Margaret V. Lanahan, Michael E. Cristel, Jason S. Lewis, and Sally W. Schwarz. "Radiotherapy, toxicity and dosimetry of copper-64-TETA-octreotide in tumor-bearing rats." Journal of Nuclear Medicine 39, no. 11 (1998): 1944-1951.

[50] Shokeen, Monica, and Carolyn J. Anderson. "Molecular imaging of cancer with copper-64 radiopharmaceuticals and positron emission tomography (PET)." Accounts of chemical research 42, no. 7 (2009): 832-841.